PAIN

Long-lasting analgesia via targeted in situ repression of $Na_V1.7$ in mice

Ana M. Moreno[1]*, Fernando Alemán[1]*, Glaucilene F. Catroli[2], Matthew Hunt[2], Michael Hu[1], Amir Dailamy[1], Andrew Pla[1], Sarah A. Woller[2†], Nathan Palmer[3], Udit Parekh[4], Daniella McDonald[1,5], Amanda J. Roberts[6], Vanessa Goodwill[7], Ian Dryden[7], Robert F. Hevner[7], Lauriane Delay[2], Gilson Gonçalves dos Santos[2], Tony L. Yaksh[2‡], Prashant Mali[1‡]

Current treatments for chronic pain rely largely on opioids despite their substantial side effects and risk of addiction. Genetic studies have identified in humans key targets pivotal to nociceptive processing. In particular, a hereditary loss-of-function mutation in $Na_V1.7$, a sodium channel protein associated with signaling in nociceptive sensory afferents, leads to insensitivity to pain without other neurodevelopmental alterations. However, the high sequence and structural similarity between Na_V subtypes has frustrated efforts to develop selective inhibitors. Here, we investigated targeted epigenetic repression of $Na_V1.7$ in primary afferents via epigenome engineering approaches based on clustered regularly interspaced short palindromic repeats (CRISPR)–dCas9 and zinc finger proteins at the spinal level as a potential treatment for chronic pain. Toward this end, we first optimized the efficiency of $Na_V1.7$ repression in vitro in Neuro2A cells and then, by the lumbar intrathecal route, delivered both epigenome engineering platforms via adeno-associated viruses (AAVs) to assess their effects in three mouse models of pain: carrageenan-induced inflammatory pain, paclitaxel-induced neuropathic pain, and BzATP-induced pain. Our results show effective repression of $Na_V1.7$ in lumbar dorsal root ganglia, reduced thermal hyperalgesia in the inflammatory state, decreased tactile allodynia in the neuropathic state, and no changes in normal motor function in mice. We anticipate that this long-lasting analgesia via targeted in vivo epigenetic repression of $Na_V1.7$ methodology we dub pain LATER, might have therapeutic potential in management of persistent pain states.

INTRODUCTION

Chronic pain affects between 19 and 50% of the world population (*1*, *2*). The high prevalence is understandable given that a continuing pain state and its associated debilitating effects on quality of life accompanies virtually every diagnosis of cancer, diabetes, and cardiovascular disease (*3*). Current standard of care for chronic pain often relies on opioids, which have adverse side effects and profound addiction risk (*4*). Despite decades of research, the goal of achieving broadly effective, long-lasting, nonaddictive therapeutics for chronic pain has remained elusive.

Pain arising from somatic or nerve injury/pathologies typically arises by activation of populations of primary afferent neurons, which are characterized by activation thresholds associated with tissue injury and by sensitivity to products released by local tissue injury and inflammation (*5*). These afferents terminate in the spinal dorsal horn, where this input is encoded and transmitted by long ascending tracts to the brain, where it is processed into the pain experience (*5*). The cell body of a primary afferent lies in its dorsal root ganglion (DRG). These neuronal cell bodies synthesize the voltage-gated sodium channels that serve to initiate and propagate the action potential (*5*). Although local anesthetics can yield a dense anesthesia, previous work has shown that nonspecific sodium channel blockers such as lidocaine delivered systemically at subanesthetic concentrations were able to have selective effects upon hyperpathia in animal models and humans (*6*, *7*).

It is now known that there are nine voltage-gated sodium channel subtypes along with numerous splice variants. Of note, three of these isotypes—$Na_V1.7$ (*8*), $Na_V1.8$ (*9*), and $Na_V1.9$ (*10*)—have been found to be principally expressed in primary afferent nociceptors and genetically associated with pain states. The relevance of these isotypes to human pain has been suggested by the observation that a loss-of-function mutation in $Na_V1.7$ (*SCN9A*) leads to congenital insensitivity to pain (CIP), a rare genetic disorder. Conversely, gain-of-function mutations yield anomalous hyperpathic states (*11*). On the basis of these observations, the $Na_V1.7$ channel has been considered an attractive target for addressing pathologic pain states and for developing chronic pain therapies (*8*, *12*, *13*). Efforts to develop selective small-molecule inhibitors have, however, been hampered because of the sequence similarity between Na_V subtypes. Many small-molecule drugs targeting $Na_V1.7$ have accordingly failed because of side effects caused by lack of targeting specificity or their limited bioavailability by the systemic route (*14*). In addition, antibodies have faced a similar situation, because there is a trade-off between selectivity and potency due to the binding of a specific (open or close) conformation of the channel, with binding not always translating into successful channel inhibition (*15*). Consequently, despite preclinical studies demonstrating that decreased $Na_V1.7$ activity leads to a reduction in inflammatory and neuropathic pain (*8*, *9*, *16*, *17*), no molecule targeting this gene product has been approved (*14*). We therefore took an alternative approach by (i) epigenetically

[1]Department of Bioengineering, University of California San Diego, San Diego, CA 92093, USA. [2]Department of Anesthesiology, University of California San Diego, San Diego, CA 92093, USA. [3]Division of Biological Sciences, University of California San Diego , San Diego, CA 92093, USA. [4]Department of Electrical Engineering, University of California San Diego , San Diego, CA 92093, USA. [5]Biomedical Sciences Graduate Program, University of California San Diego, San Diego, San Diego, CA 92093, USA. [6]Animal Models Core, Scripps Research Institute, La Jolla, CA 92037, USA. [7]Department of Neuropathology, University of California San Diego, San Diego, CA 92093, USA.
*Present address: Navega Therapeutics, San Diego, CA 92121, USA.
†Present address: National Institutes of Neurological Disorder and Stroke, National Institutes of Health, Bethesda, MD 20852, USA.
‡Corresponding author. Email: pmali@ucsd.edu (P.M.); tyaksh@ucsd.edu (T.L.Y.)

modulating the expression of $Na_V1.7$ using two genome engineering tool variants, clustered regularly interspaced short palindromic repeats-Cas9 (CRISPR-Cas9) and zinc finger proteins (ZFPs), such that one could engineer highly specific, long-lasting, and reversible treatments for pain and (ii) targeting spinal $Na_V1.7$ signaling through intrathecal delivery where considerable work has shown that viral vectors result in local effects upon the DRG cell body of the afferent neurons (*18*–*20*).

Through its ability to precisely target pathology-causing DNA mutations, the CRISPR-Cas9 system has emerged as a potent tool for genome manipulation and has shown therapeutic efficacy in multiple animal models of human diseases (*21*). However, permanent genome editing, leading to permanent alteration of pain perception, may not be desirable. For these reasons, we have used a catalytically inactivated "dead" Cas9 (dCas9; also known as CRISPRi), which does not cleave DNA but maintains its ability to bind to the genome via a guide RNA (gRNA), and fused it to a repressor domain [Krüppel-associated box (KRAB)] to enable nonpermanent gene repression of $Na_V1.7$. Previously, we and others have shown that through addition of a KRAB epigenetic repressor motif to dCas9, gene repression can be enhanced with a high level of specificity both in vitro (*22*, *23*) and in vivo (*24*, *25*). This transcriptional modulation system takes advantage of the high specificity of CRISPR-Cas9 while simultaneously increasing the safety profile, because no permanent modification of the genome is performed. As a second approach for in situ epigenome repression of $Na_V1.7$, we also used Zinc-Finger-KRAB proteins (ZFP-KRAB), consisting of a DNA binding domain made up of Cys_2His_2 zinc fingers fused to a KRAB repressor. ZFPs constitute the largest individual family of transcriptional modulators encoded by the genomes of higher organisms (*26*) and, with prevalent synthetic versions engineered on human protein chasses, present a potentially low immunogenicity in vivo targeting approach (*27*–*29*). We sought to produce a specific anatomic targeting of the gene regulation by delivering both epigenetic tools in an adeno-associated virus (AAV) construct into the spinal intrathecal space. This approach has several advantages as it permits the use of minimal viral loads and reduces the possibility of systemic immunogenicity.

Because pain perception is etiologically diverse and multifactorial, several rodent pain models have been used to study pain signaling and pain behaviors (*30*). In the present work, we sought to characterize the effects of CRISPR-dCas9 and ZFP-mediated knockdown of $Na_V1.7$ using three mechanistically distinct models: (i) thermal sensitivity in control (normal) and unilateral inflammation-sensitized hind paw, (ii) a polyneuropathy induced by a chemotherapeutic yielding a bilateral hind paw tactile allodynia, and (iii) a spinally evoked bilateral hind paw tactile allodynia induced by the spinal activation of purine receptors. Pain due to tissue injury and inflammation results from a release of factors that sensitize the peripheral terminal of the nociceptive afferent neuron. This phenotype can be studied through local application of carrageenan to the paw resulting in inflammation, swelling, increased expression of $Na_V1.7$ (*31*), and a robust increase in thermal and mechanical sensitivity (hyperalgesia) (*32*). Chemotherapy to treat cancer often leads to a polyneuropathy characterized by increased sensitivity to light touch (tactile allodynia) and cold. Paclitaxel is a commonly used chemotherapeutic that increases the expression of Na_V 1.7 in the nociceptive afferents (*33*) and induces a robust allodynia in animal models (*34*). Last, ATP (adenosine triphosphate) by an action on a variety of purine receptors expressed on afferent terminals and second-order neurons and nonneuronal cells has been broadly implicated in inflammatory, visceral, and neuropathic pain states (*35*). Thus, intrathecal delivery of a stable ATP analog [2′,3′-*O*-(4-benzoylbenzoyl)-ATP (BzATP)] results in a long-lasting allodynia in mice (*36*).

Our results show that the in vivo repression of $Na_V1.7$ leads to a decrease in thermal hyperalgesia in a carrageenan pain model. Similarly, the results in the paclitaxel-induced neuropathic pain model indicate that repression of $Na_V1.7$ leads to reduced tactile and cold allodynia. In addition, KRAB-dCas9–injected mice showed reduced tactile allodynia after administration of the ATP analog BzATP. Last, we demonstrated the efficacy of our epigenome strategy in reversing an established chemotherapy-induced neuropathic pain state—relevant to the clinical setting. As many pain states occurring after chronic inflammation and nerve injury represent an enduring condition, typically requiring constant remedication, these genetic approaches provide ongoing and controllable regulation of this aberrant processing. Overall, these in situ epigenetic approaches represent a viable replacement strategy for opioids and serve as a potential therapeutic approach for long-lasting chronic pain.

RESULTS

In vitro optimization

With the goal of developing a therapeutic product that relieves chronic pain in a nonpermanent, nonaddictive, and long-lasting manner, we explored the use of two independent genetic approaches to inhibit the transmission of pain at the spinal level (Fig. 1). To establish robust $Na_V1.7$ repression, we first compared in vitro repression efficacy of $Na_V1.7$ using KRAB-dCas9 and ZFP-KRAB AAV vector constructs (fig. S1, A and B). Because of the limited packaging capacity of AAVs (~4.7 kb), which does not typically accommodate the payload requirements of delivering a dCas9, the associated gRNA, and KRAB domain for genome repression, we used our previously developed dual-AAV split-dCas9 platform (*24*) in which the *Streptococcus pyogenes* dCas9 is split into two fragments: an N-terminal dCas9 fused to an N-intein and a C-terminal dCas9 fused to a C-intein (fig. S1A). Toward this, we cloned 10 gRNAs (table S1) that target $Na_V1.7$ close to the transcriptional start site (TSS). We also cloned the two gRNAs that were predicted to have the highest efficiency (SCN9A-1 and SCN9A-2) into a single construct, because we have previously shown that higher efficacy can be achieved by using multiple gRNAs (*24*). We next evaluated four ZFP-KRAB constructs targeting the $Na_V1.7$ DNA sequence close to the TSS (table S2). We transfected these constructs into a mouse neuroblastoma cell line that expresses $Na_V1.7$ (Neuro2a) and confirmed repression of $Na_V1.7$ relative to glyceraldehyde-3-phosphate dehydrogenase (Gapdh) with quantitative polymerase chain reaction (qPCR). Six of 10 gRNAs repressed the $Na_V1.7$ transcript by >50% compared to the nontargeting gRNA control, with gRNA-2 being the single gRNA having the highest repression (56%; $P < 0.0001$) and with the dual gRNA having the highest overall repression (71%; $P < 0.0001$), which we used for subsequent in vivo studies (fig. S1C). Of the ZFP-KRAB designs, the Zinc-Finger-4-KRAB construct had the highest repression (88%; $P < 0.0001$) compared to the negative control (mCherry), which we chose for subsequent in vivo studies (fig. S1C).

In vivo evaluation of AAV9 mCherry DRG transduction along the neuraxis

As a first approach to test AAV9 transduction efficacy of sensory neurons in the DRG, we delivered 1×10^{10}, 1×10^{11}, or 1×10^{12} viral

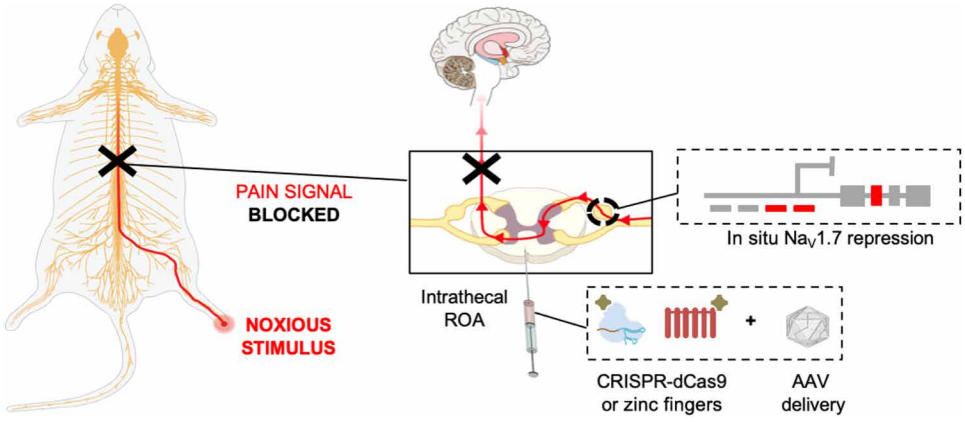

Fig. 1. Schematic of the overall strategy used for in situ $Na_V1.7$ repression using ZFP-KRAB and KRAB-dCas9 via the intrathecal route of administration (ROA). $Na_V1.7$ is a DRG channel involved in the transduction of noxious stimuli into electric impulses at the peripheral terminals of DRG neurons. In situ repression of $Na_V1.7$ via AAV-ZFP-KRAB and AAV-KRAB-dCas9 is achieved through intrathecal injection, leading to disruption of the pain signal before reaching the brain.

genomes (vg) per mouse of AAV9-mCherry into the cerebral spinal fluid by lumbar puncture into the subarachnoid space. Animals were euthanized 3 weeks after AAV administration, and DRGs along the neuraxis (cervical, thoracic, lumbar, and sacral) were harvested. Native mCherry expression was visualized by direct whole-cell mount fluorescent confocal imaging, and the neuraxial distribution of small, medium, and large DRG neuronal soma as a function of their average soma fluorescent intensity was quantified (Fig. 2, A and B, and fig. S2, A and B). We found that the intrathecal delivery of AAV9, which has neuronal tropism (*37*), serves to efficiently target the DRG. Mice injected with a fixed volume (5 μl) of AAV titers of 1×10^{12}, 1×10^{11}, or 1×10^{10} vg per mouse revealed a titer-dependent increase in lumbar DRG transduction, with no notable difference between the 1×10^{10} and 1×10^{11} vg per mouse injected mice and with a significant increase in transduction efficacy in the 1×10^{12} vg per mouse injected group ($P < 0.0001$). Transduction of thoracic and cervical DRG was observed in the 1×10^{12} injected mice ($P = 0.0224$ and $P = 0.0384$, respectively), but not in the 1×10^{10} or 1×10^{11} injected mice, indicating a viral load sufficient to result in robust AAV9-mCherry transduction along the neuraxis. Thus, we chose 5 μl of 1×10^{12} vg per mouse as our titer per dosage for subsequent experiments.

$Na_V1.7$ repression

Next, we performed RNAscope hybridization on mice DRGs transduced with 1×10^{12} vg per mouse of AAV9-mCherry or AAV9-Zinc-Finger-4-KRAB to assess the in situ down-regulation of $Na_V1.7$ in lumbar DRG. The amount of $Na_V1.7$ expression in the negative control (AAV9-mCherry) was significantly higher than in AAV9-Zinc-Finger-4-KRAB–injected mice ($P = 0.0205$) (Fig. 2, C to E).

In vivo evaluation in a carrageenan model of inflammatory pain

We next focused on testing the effectiveness of the best ZFP-KRAB and KRAB-dCas9 constructs from the in vitro screens (Zinc-Finger-4-KRAB and KRAB-dCas9-dual-gRNA) in a carrageenan-induced model of inflammatory pain. Mice were intrathecally injected with 1×10^{12} vg per mouse of AAV9-mCherry (negative control; $n = 10$), AAV9-Zinc-Finger-4-KRAB ($n = 10$), AAV9-KRAB-dCas9-no-gRNA (negative control; $n = 10$), and AAV9-KRAB-dCas9-dual-gRNA ($n = 10$). After 21 days, thermal pain sensitivity was measured to establish a baseline response threshold. Inflammation was induced in all four groups of mice by injecting one hind paw with carrageenan (ipsilateral), whereas the other hind paw (contralateral) was injected with saline to serve as an in-mouse control. Mice were then tested for thermal pain sensitivity at 30 min and 1, 2, 4, and 24 hours after carrageenan injection (Fig. 3A). The mean paw withdrawal latencies (PWLs) were calculated for both carrageenan- and saline-injected paws (Fig. 3, B and C), and the area under the curve (AUC) for the total mean PWL was calculated (Fig. 3D). As expected, compared to saline-injected paws, carrageenan-injected paws developed thermal hyperalgesia, measured by a decrease in PWL after application of a thermal stimulus (Fig. 3D). We also observed a significant increase in PWL in mice injected with either AAV9-Zinc-Finger-4-KRAB or AAV9-KRAB-dCas9-dual-gRNA ($P < 0.0001$), indicating that the repression of $Na_V1.7$ in mouse DRG leads to lower thermal hyperalgesia in an inflammatory pain state. The thermal latency of the control (uninflamed paw) was not different across AAV treatment groups, indicating that the knockdown of the $Na_V1.7$ had minimal effect upon normal thermal sensitivity. Twenty-four hours after carrageenan administration, mice were euthanized and DRGs (L4 to L6) were extracted. The repression of $Na_V1.7$ transcript expression was determined by qPCR, and a significant repression of $Na_V1.7$ was observed in mice injected with AAV9-Zinc-Finger-4-KRAB (67%; $P = 0.0008$) compared to mice injected with AAV9-mCherry and in mice injected with AAV9-KRAB-dCas9-dual-gRNA (50%; $P = 0.0033$) compared to mice injected with AAV9-KRAB-dCas9-no-gRNA (Fig. 3E). As an index of edema/inflammation, we measured the ipsilateral and contralateral paws with a caliper before and 4 hours after carrageenan injection, which is the time point with the highest thermal hyperalgesia. We observed significant edema formation in both experimental and control groups ($P < 0.0001$) (fig. S2C).

Benchmarking with established small-molecule drug gabapentin

To further validate the efficacy of ZFP-KRAB in ameliorating thermal hyperalgesia in a carrageenan model of inflammatory pain, we next conducted a separate experiment and tested the small-molecule drug gabapentin as a positive control. Mice were intrathecally injected with 1×10^{12} vg per mouse of AAV9-mCherry ($n = 5$), AAV9-Zinc-Finger-4-KRAB ($n = 6$), or saline ($n = 5$). After 21 days, thermal nociception was measured in all mice as previously described. One hour before carrageenan administration, the mice that received intrathecal saline were injected as a positive comparator with intraperitoneal gabapentin (100 mg/kg). This agent is known to reduce carrageenan-induced thermal hyperalgesia in rodents through binding to spinal alpha2 delta subunit of the voltage-gated calcium channel (*38*, *39*). Twenty-four hours after carrageenan administration,

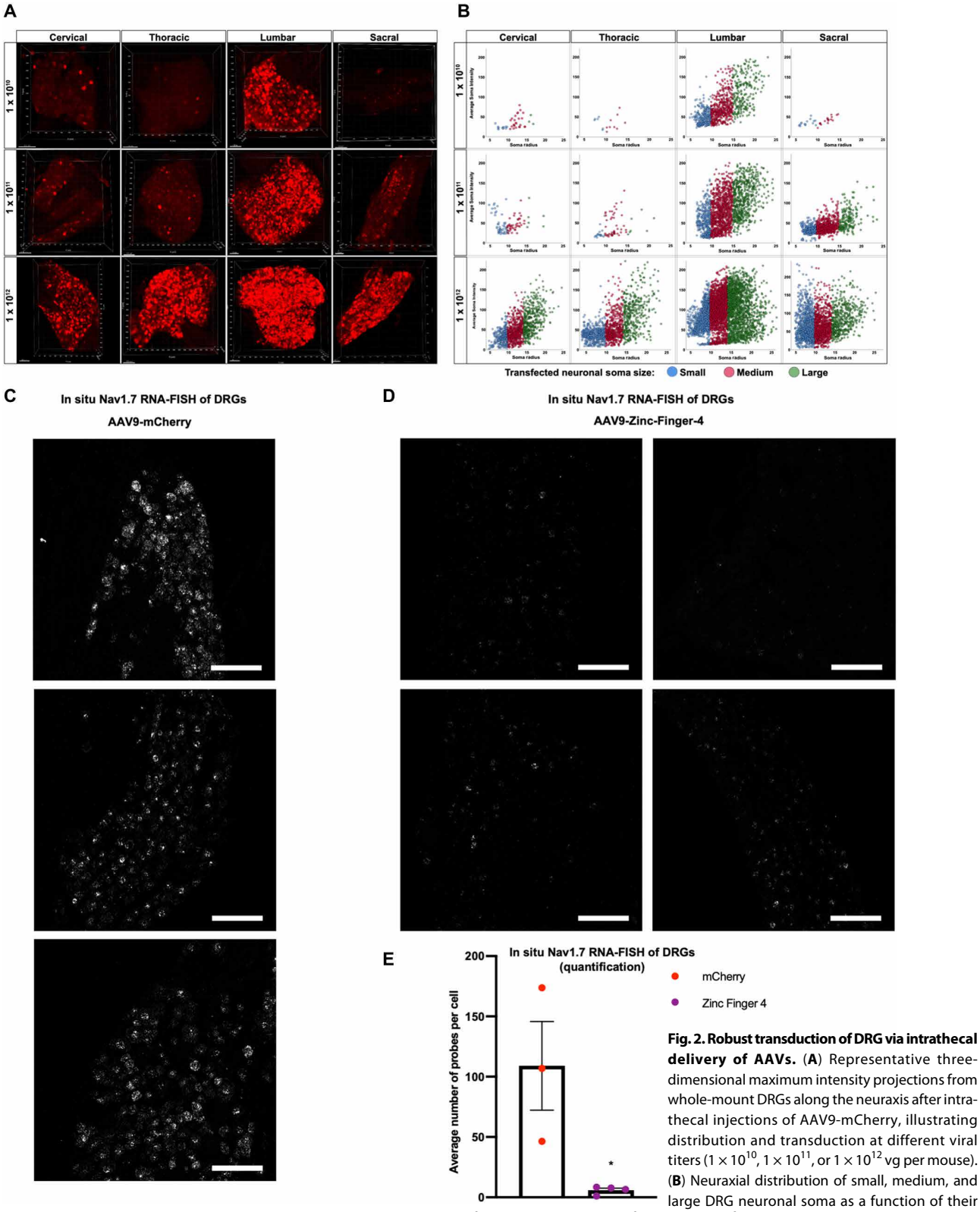

Fig. 2. Robust transduction of DRG via intrathecal delivery of AAVs. (**A**) Representative three-dimensional maximum intensity projections from whole-mount DRGs along the neuraxis after intrathecal injections of AAV9-mCherry, illustrating distribution and transduction at different viral titers (1×10^{10}, 1×10^{11}, or 1×10^{12} vg per mouse). (**B**) Neuraxial distribution of small, medium, and large DRG neuronal soma as a function of their average soma fluorescent intensity ($n = 4$ mice per titer; cross-sectional area: small $\leq 300\ \mu m^2$, medium = 300 to $700\ \mu m^2$, large $\geq 700\ \mu m^2$). (**C** and **D**) Representative 20× images of mice DRG transduced with 1×10^{12} vg per mouse of AAV9-mCherry (C) or AAV9-Zinc-Finger-4-KRAB (D) labeled with RNAscope in situ hybridization for $Na_V1.7$ ($n = 3$ for mCherry and $n = 4$ for Zinc-Finger-4-KRAB; scale bar, 50 μm). (**E**) Quantification of $Na_V1.7$ expression in AAV9-mCherry or AAV9-Zinc-Finger-4-KRAB treatment conditions: Individual RNAscope probes and cells were identified in each respective image and used to calculate the average number of probes per cell (dots represent individual biological replicates; $n = 3$ for mCherry and $n = 4$ for Zinc-Finger-4-KRAB; error bars are SEM; Student's t test, $^*P = 0.0205$).

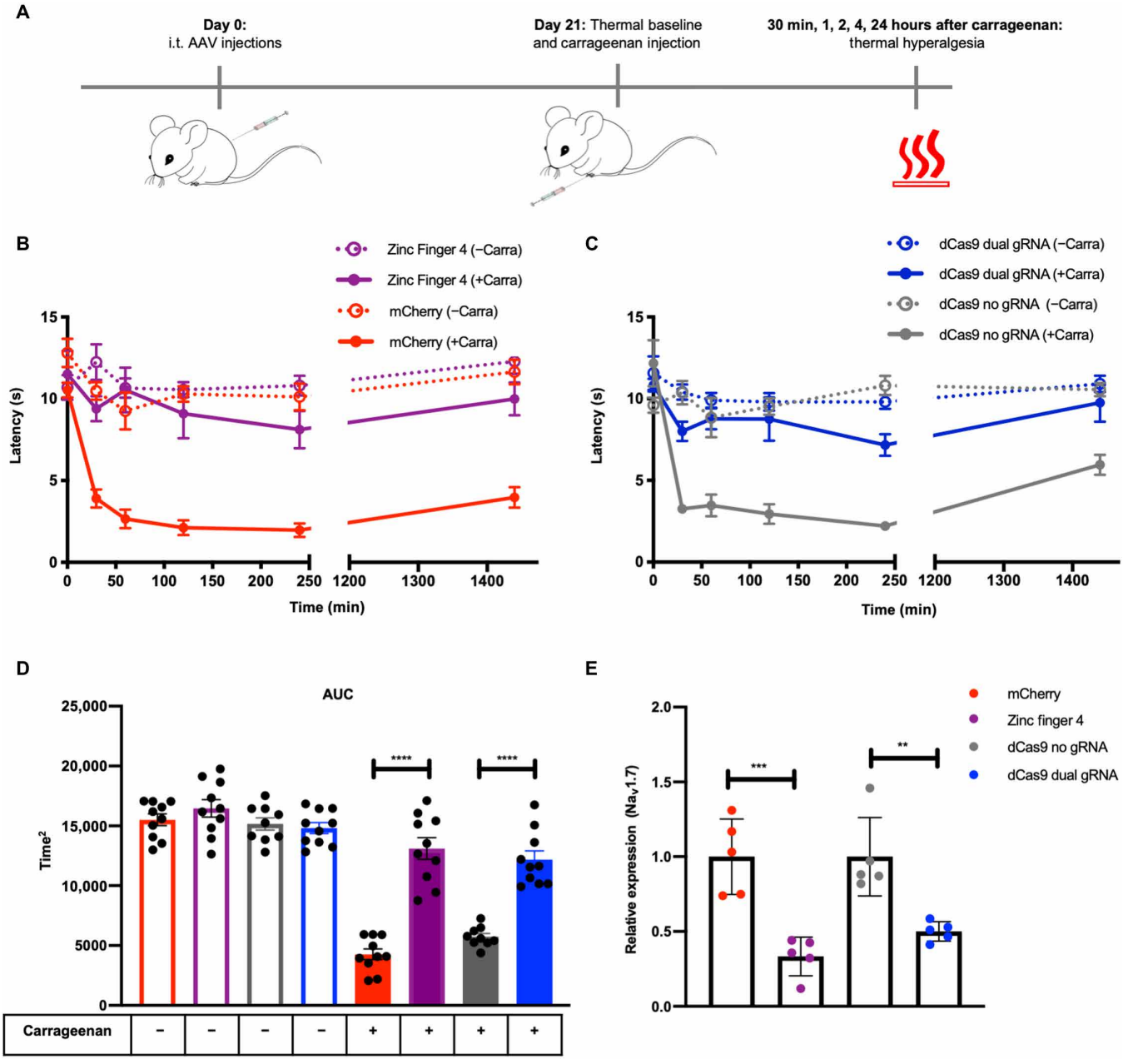

Fig. 3. In situ repression of $Na_V1.7$ leads to pain prevention in a carrageenan model of inflammatory pain. (**A**) Schematic of the carrageenan-induced inflammatory pain model. (**B**) Time course of thermal hyperalgesia after the injection of carrageenan (solid lines) or saline (dotted lines) into the hind paw of mice 21 days after intrathecal (i.t.) injection with AAV9-mCherry and AAV9-Zinc-Finger-4-KRAB is plotted. Mean PWLs are shown (dots represent mean of individual biological replicates; $n = 10$; error bars are SEM). (**C**) Time course of thermal hyperalgesia after the injection of carrageenan (solid lines) or saline (dotted lines) into the hind paw of mice 21 days after intrathecal injection with AAV9-KRAB-dCas9-no-gRNA and AAV9-KRAB-dCas9-dual-gRNA is plotted. Mean PWLs are shown ($n = 10$; error bars are SEM). (**D**) The aggregate PWL was calculated as AUC for both carrageenan- and saline-injected paws (dots represent individual biological replicates; $n = 10$; error bars are SEM; Student's t test, $^{****}P < 0.0001$). (**E**) In vivo $Na_V1.7$ repression efficiencies as determined by qPCR (dots represent individual biological replicates; qPCR was performed in technical triplicates; $n = 5$; error bars are SEM; values normalized to Gapdh; Student's t test, $^{***}P = 0.0008$ and $^{**}P = 0.0033$).

mice were euthanized and DRGs (L4 to L6) were extracted. The repression of $Na_V1.7$ transcript expression was determined by qPCR, and a significant repression of $Na_V1.7$ was observed in AAV9-Zinc-Finger-4-KRAB ($P = 0.0007$) and gabapentin groups ($P = 0.0121$) (fig. S3A). The mean PWL was calculated for both carrageenan- and saline-injected paws. We then calculated the AUC for thermal hyperalgesia. We observed a significant increase in PWL in the carrageenan-injected gabapentin group (39% improvement, $P = 0.0208$) (fig. S3B) and in the AAV9-Zinc-Finger-4-KRAB group (115% improvement, $P = 0.0021$) (fig. S3C) compared to the carrageenan-injected AAV9-mCherry control. Last, we compared PWLs of carrageenan-injected paws for AAV9-Zinc-Finger-4-KRAB and

gabapentin groups at each time point to the AAV9-mCherry carrageenan-injected control using a two-way analysis of variance (ANOVA) calculation to determine whether there was any reduction in thermal hyperalgesia (fig. S3D). When comparing carrageenan-injected hind paws, we observed that only AAV9-Zinc-Finger-4-KRAB had significantly higher PWL at all the time points after carrageenan injection when compared to the AAV9-mCherry control ($P < 0.0001$ after 30 min, $P = 0.0002$ after 1 hour, $P < 0.0001$ after 2 hours, $P = 0.0104$ after 4 hours, and $P = 0.0028$ after 24 hours). We also observed significance in PWL for the gabapentin-positive control group at the 30-min ($P = 0.0081$), 1-hour ($P = 0.0276$), and 4-hour ($P = 0.0184$) time points, but not at the 24-hour time point. This result reflects the half-life of gabapentin (3 to 5 hours). Of note, the thermal escape latency of the contralateral noninflamed paw showed no difference among groups.

In vivo repression of $Na_V1.7$ prevents chronic pain in a polyneuropathic pain model

After having established in vivo efficacy in an inflammatory pain model, we next evaluated our epigenome repression strategy for neuropathic pain using the polyneuropathy produced by the chemotherapeutic paclitaxel. To establish this model, mice were first injected with 1×10^{12} vg per mouse of AAV9-mCherry ($n = 8$), AAV9-Zinc-Finger-4-KRAB ($n = 8$), AAV9-KRAB-dCas9-dual-gRNA ($n = 8$), AAV9-KRAB-dCas9-no-gRNA ($n = 8$), or saline ($n = 16$). Fourteen days later and before paclitaxel administration, we established a baseline for tactile threshold (von Frey filaments). Mice were then administered with intraperitoneal paclitaxel at days 14, 16, 18, and 20, with a dosage of 8 mg/kg (total cumulative dosage of 32 mg/kg), with a group of saline-injected mice not receiving any paclitaxel ($n = 8$) to establish the tactile allodynia caused by the chemotherapeutic. Twenty-one days after the initial injections and 1 hour before testing, a group of saline-injected mice ($n = 8$) were injected with intraperitoneal gabapentin (100 mg/kg). Mice were then tested for tactile allodynia via von Frey filaments and for cold allodynia via acetone testing (Fig. 4A). A 50% tactile threshold was calculated. We observed a decrease in tactile threshold in mice receiving AAV9-mCherry and AAV9-KRAB-dCas9-no-gRNA, whereas mice that received gabapentin, AAV9-Zinc-Finger-4-KRAB ($P = 0.0007$), and AAV9-KRAB-dCas9-dual-gRNA ($P = 0.0004$) had increased withdrawal thresholds, indicating that in situ $Na_V1.7$ repression can prevent chemotherapy-induced tactile allodynia (Fig. 4B). Similarly, an increase in the number of withdrawal responses is seen in mice tested for cold allodynia in the negative control groups (AAV9-mCherry and AAV9-KRAB-dCas9-no-gRNA), whereas both AAV9-Zinc-Finger-4-KRAB ($P < 0.0001$) and AAV9-KRAB-dCas9-dual-gRNA ($P = 0.008$) groups had a decrease in withdrawal responses, indicating that in situ repression of $Na_V1.7$ also leads to a decrease in chemotherapy-induced cold allodynia (Fig. 4C).

In vivo repression of $Na_V1.7$ decreases mechanical allodynia in a model of spinally evoked nociception

We next tested whether in situ repression of $Na_V1.7$ via KRAB-dCas9 could prevent neuropathic pain in another model and specifically focused on BzATP-induced pain. This molecule activates P2X receptors located on central terminals, leading to a centrally mediated hyperalgesic state. We first injected mice with 1×10^{12} vg per mouse of AAV9-mCherry ($n = 6$), AAV9-KRAB-dCas9-no-gRNA ($n = 5$), and AAV9-KRAB-dCas9-dual-gRNA ($n = 6$). After 21 days, tactile thresholds were determined with von Frey filaments, and mice were injected intrathecally with BzATP (30 nmol). Tactile allodynia was then measured at 30 min and 1, 2, 3, 6, and 24 hours after BzATP administration (Fig. 4D). We observed a significant decrease in tactile allodynia at 30-min ($P < 0.0001$), 1-hour ($P < 0.0001$), and 3-hour ($P = 0.0469$) time points in mice injected with AAV9-KRAB-dCas9-dual-gRNA, and an overall increase in tactile threshold at all time points (Fig. 4E).

In vivo repression of $Na_V1.7$ reverses chronic pain in a polyneuropathic pain model

After establishing that in situ $Na_V1.7$ repression can prevent hyperalgesia in three different pain models, we next tested this approach in an established chemotherapy-induced neuropathic pain state to determine whether epigenetic repression could reverse mechanical allodynia. To establish this model, we first performed a baseline for tactile threshold (von Frey filaments). We then intraperitoneally injected mice ($n = 54$) with paclitaxel at days 1, 3, 5, and 7, with a dosage of 8 mg/kg (total cumulative dosage of 32 mg/kg), whereas a group of mice ($n = 8$) was intraperitoneally injected with saline to establish the tactile allodynia caused by the chemotherapeutic. After confirming paclitaxel-induced tactile allodynia, we intrathecally injected mice with 1×10^{12} vg per mouse of AAV9-mCherry ($n = 8$), AAV9-Zinc-Finger-4-KRAB ($n = 8$), AAV9-KRAB-dCas9-no-gRNA ($n = 7$), AAV9-KRAB-dCas9-gRNA ($n = 7$), or saline ($n = 16$). In addition, as both 1×10^{11} and 1×10^{12} vg per mouse of AAV9-mCherry demonstrated robust lumbar DRG transduction (Fig. 2, A and B) and to determine whether a 10-fold decrease in viral titer would be efficacious in ameliorating pain, we intrathecally injected two groups of mice with 1×10^{11} vg per mouse of AAV9-mCherry ($n = 8$) or AAV9-Zinc-Finger-4-KRAB ($n = 8$). Twenty-one and 28 days after, mice were tested for tactile allodynia via von Frey filaments, with one group of saline-injected mice ($n = 8$) injected with intraperitoneal gabapentin (100 mg/kg) 1 hour before testing (Fig. 5A). A 50% tactile threshold was calculated. We observed a significant decrease in tactile allodynia for mice injected with AAV9-Zinc-Finger-4-KRAB at 21 days after AAV9 injections ($P = 0.0028$ for 1×10^{11} vg dose; $P < 0.0001$ for 1×10^{12} vg dose) and at 28 days after AAV9 injection ($P < 0.0001$ for both 1×10^{11} and 1×10^{12} vg doses). In addition, we observed a significant decrease in tactile allodynia for AAV9-KRAB-dCas9-gRNA gRNA–injected mice at both 21 and 28 days after AAV9 injections ($P < 0.0001$) (Fig. 5B).

Durable in situ repression of $Na_V1.7$ for pain prevention

To determine whether in situ repression of $Na_V1.7$ was efficacious long term, we repeated the carrageenan inflammatory pain model and tested thermal hyperalgesia at 42, 84, and 308 days after intrathecal AAV injection ($n = 5$ to 8 per group) (Fig. 6A). We observed a significant improvement in PWL for carrageenan-injected paws in AAV9-Zinc-Finger-4-KRAB groups at all three time points ($P < 0.0001$) (Fig. 6B), demonstrating the durability of this approach. To determine whether in situ repression of $Na_V1.7$ was also efficacious long term in a polyneuropathic pain model, we measured tactile and cold allodynia 105 days after initial AAV injections and 85 days after the last paclitaxel injection (total cumulative dosage of 32 mg/kg; Fig. 6C). Compared to the earlier time point (Fig. 4B), we observed that mice from both AAV9-mCherry ($n = 8$) and AAV9-KRAB-dCas9-no-gRNA ($n = 6$) groups had increased tactile allodynia at day 105 as compared to day 21 and responded to the lowest

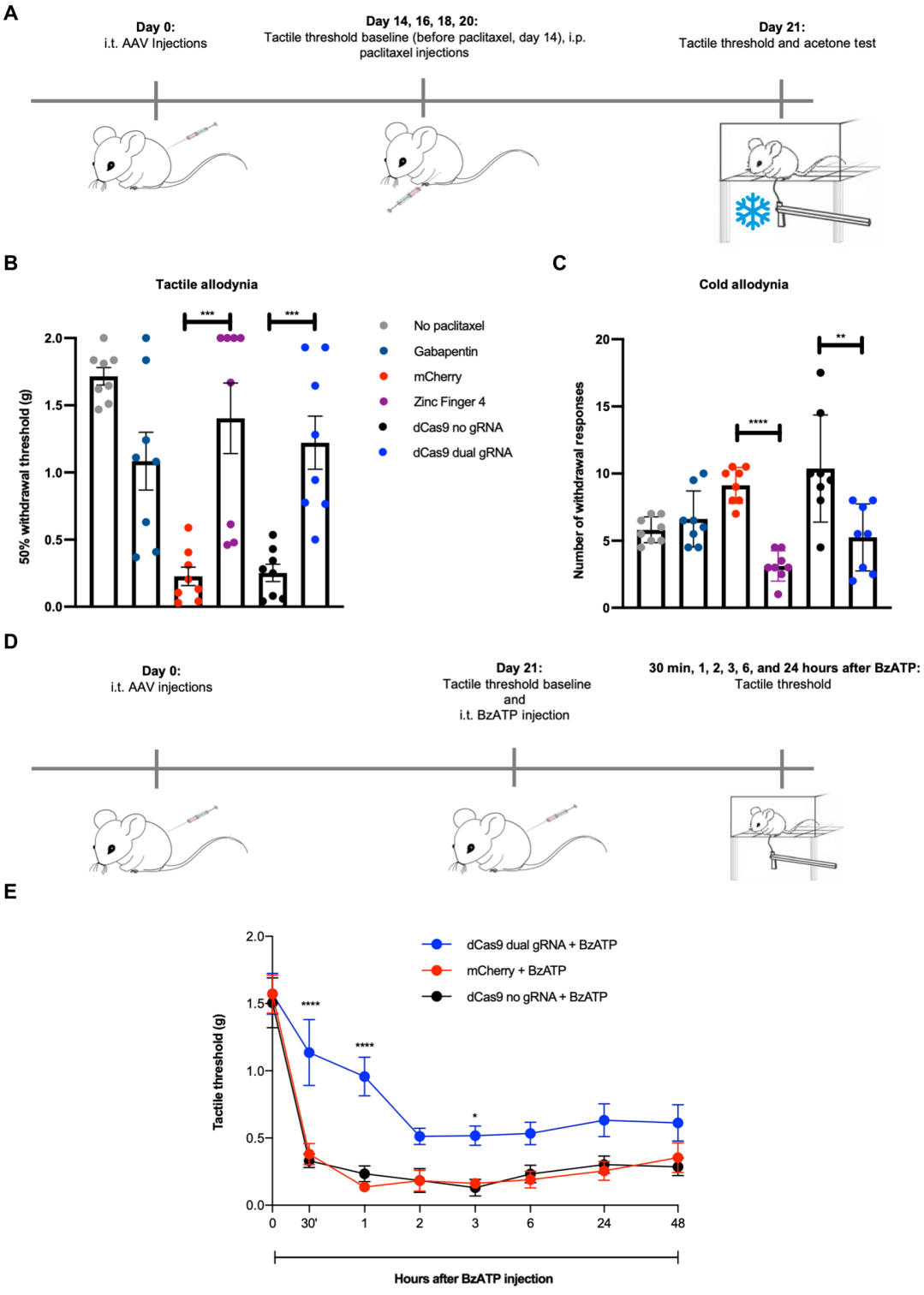

Fig. 4. In vivo efficacy of ZFP-KRAB and KRAB-dCas9 in two neuropathic pain models. (**A**) Schematic of the paclitaxel-induced neuropathic pain model. i.p., intraperitoneally. (**B**) In situ repression of $Na_V1.7$ via Zinc-Finger-4-KRAB and KRAB-dCas9-dual-gRNA reduces paclitaxel-induced tactile allodynia (dots represent individual biological replicates; $n = 8$; error bars are SEM; Student's t test, $^{***}P = 0.0007$ and $^{***}P = 0.0004$). (**C**) In situ repression of $Na_V1.7$ via Zinc-Finger-4-KRAB and KRAB-dCas9-dual-gRNA reduces paclitaxel-induced cold allodynia (dots represent individual biological replicates; $n = 8$; error bars are SEM; Student's t test, $^{****}P < 0.0001$ and $^{**}P = 0.008$). (**D**) Schematic of the BzATP pain model. (**E**) In situ repression of $Na_V1.7$ via KRAB-dCas9-dual-gRNA reduces tactile allodynia in a BzATP model of neuropathic pain (dots represent mean of $n = 5$ biological replicates for KRAB-dCas9-no-gRNA and $n = 6$ biological replicates for the other groups; error bars are SEM; two-way ANOVA with Bonferroni post hoc test, $^{****}P < 0.0001$ and $^{*}P = 0.0469$).

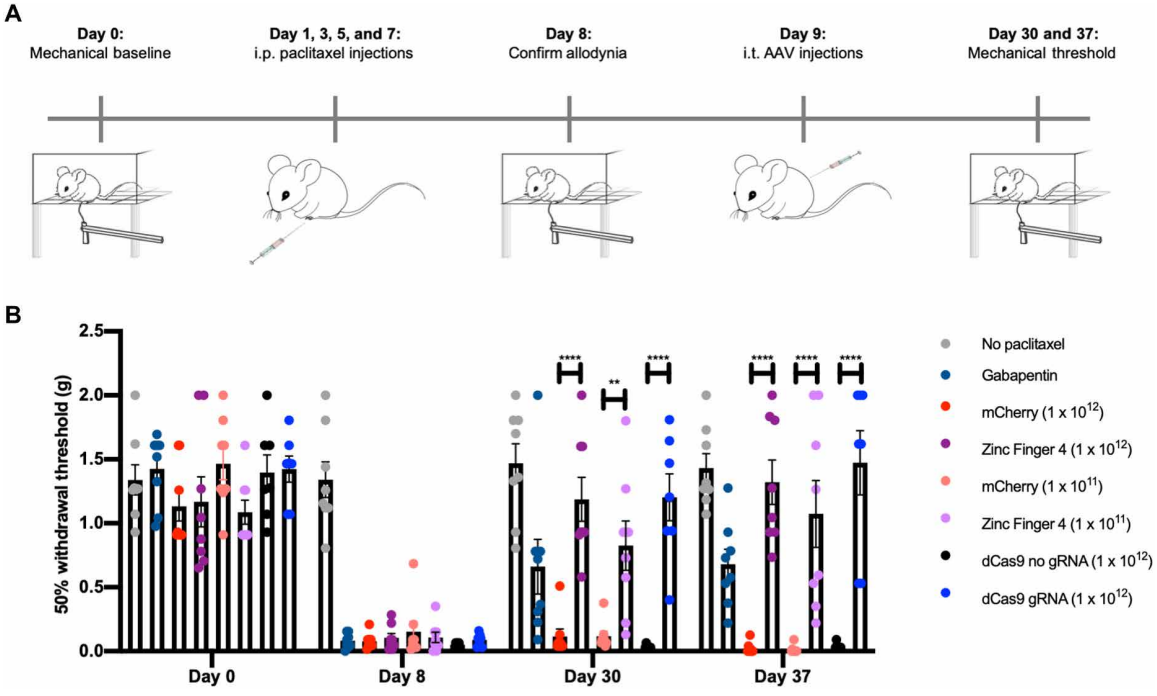

Fig. 5. In situ repression of $Na_V1.7$ reverses chemotherapy-induced neuropathic pain. (**A**) Schematic of the treatment for paclitaxel-induced chronic neuropathic pain model. (**B**) In situ repression of $Na_V1.7$ via Zinc-Finger-4-KRAB and KRAB-dCas9-gRNA reverses paclitaxel-induced tactile allodynia (dots represent individual biological replicates; $n = 7$ to 8; error bars are SEM; two-way ANOVA with Bonferroni post hoc test, $^{****}P < 0.0001$ and $^{**}P = 0.0027$).

von Frey filament examined (0.04 g). In comparison, mice receiving AAV9-Zinc-Finger-4-KRAB ($n = 5$; $P < 0.0001$) and AAV9-KRAB-dCas9-dual-gRNA ($n = 7$; $P < 0.0001$) had increased withdrawal thresholds, indicating that in situ $Na_V1.7$ repression leads to long-term prevention in chemotherapy-induced tactile allodynia (Fig. 6D). As before, an increase in the number of withdrawal responses is seen in mice tested for cold allodynia in the negative control groups (AAV9-mCherry and AAV9-KRAB-dCas9-no-gRNA), while both AAV9-Zinc-Finger-4-KRAB and AAV9-KRAB-dCas9-dual-gRNA groups had a decrease in withdrawal responses ($P < 0.0001$), indicating that in situ repression of $Na_V1.7$ also leads to long-term prevention of chemotherapy-induced cold allodynia (Fig. 6E).

Safety and specificity analysis of ZFP-KRAB and KRAB-dCas9

To determine potential side effects of $Na_V1.7$ epigenetic repression via ZFP-KRAB and KRAB-dCas9, we performed a series of toxicity/side effect tests for examination of general health and behavior in mice. These tests evaluated changes in self-care, increases in distress/stress, and illness. For these, we intrathecally injected mice with 1×10^{12} vg per mouse of AAV9-mCherry ($n = 8$), AAV9-Zinc-Finger-4-KRAB ($n = 8$), AAV9-KRAB-dCas9-no-gRNA ($n = 7$), or AAV9-KRAB-dCas9-dual-gRNA ($n = 7$). We then examined the mice 8 to 12 weeks after intrathecal injection for piloerection, arousal, muscle tone, as well as body weight and body temperature (fig. S4, A and B). The findings suggest that $Na_V1.7$ epigenetic repression via dCas9 or zinc fingers has no general effects upon nonnociresponsive behaviors (fig. S4). To determine whether there was any change in motor function, we performed a rotarod balancing test (see Materials and Methods) (*40*). We found no changes in the time to fall (fig. S4C). We also measured grip strength and found no changes in grip strength (fig. S4D).

Next, we performed a marble burying test to assess anxiety-like and possibly obsessive-compulsive–like behavior (see Materials and Methods). We found no changes in the number of marbles buried (fig. S4E). To determine whether mice maintained social behaviors, we also performed a nest building test in which nestlet material is placed in each cage, and nests are assessed at 2, 4, 6, 8, and 24 hours on a rating scale of 1 to 5 based on nest construction (*41*). We found no changes in the nest construction (fig. S4F). As loss-of-function $Na_V1.7$ mutations in individuals with CIP have anosmia (*42*), we performed an olfactory test, which examines the ability of the mice to locate a desired food item, visible or buried under bedding. We found no changes in the time to eat the desired food item for AAV9-Zinc-Finger-4-KRAB– or AAV9-KRAB-dCas9-dual-gRNA gRNA–injected mice (fig. S4G) as compared to the controls, indicating no loss of function via epigenetic repression of $Na_V1.7$. Last, we performed a cognitive test to determine whether any cognitive side effects were seen using a novel object recognition test (see Materials and Methods). We found no changes in memory retention (fig. S4H).

Next, we examined the histopathology of the DRG in the gene therapy–treated mice. We intrathecally injected C57BL/6J male mice with 1×10^{10}, 1×10^{11}, or 1×10^{12} vg per mouse of AAV9-mCherry ($n = 3$ per titer) or AAV9-Zinc-Finger-4-KRAB ($n = 3$ per titer) and harvested DRG 21 days after intrathecal treatment. Hematoxylin and eosin (H&E)–stained paraffin sections (blinded to experimental condition) were reviewed independently by three neuropathologists (fig. S5A). As expected, all specimens consisted of peripheral nerve and ganglion, with variable small amounts of bone, marrow, skeletal muscle, and fat. None of the nerves and ganglia showed axon degeneration, neuron loss, or myelin loss. In one specimen, several DRG neurons contained pale amphophilic intracytoplasmic

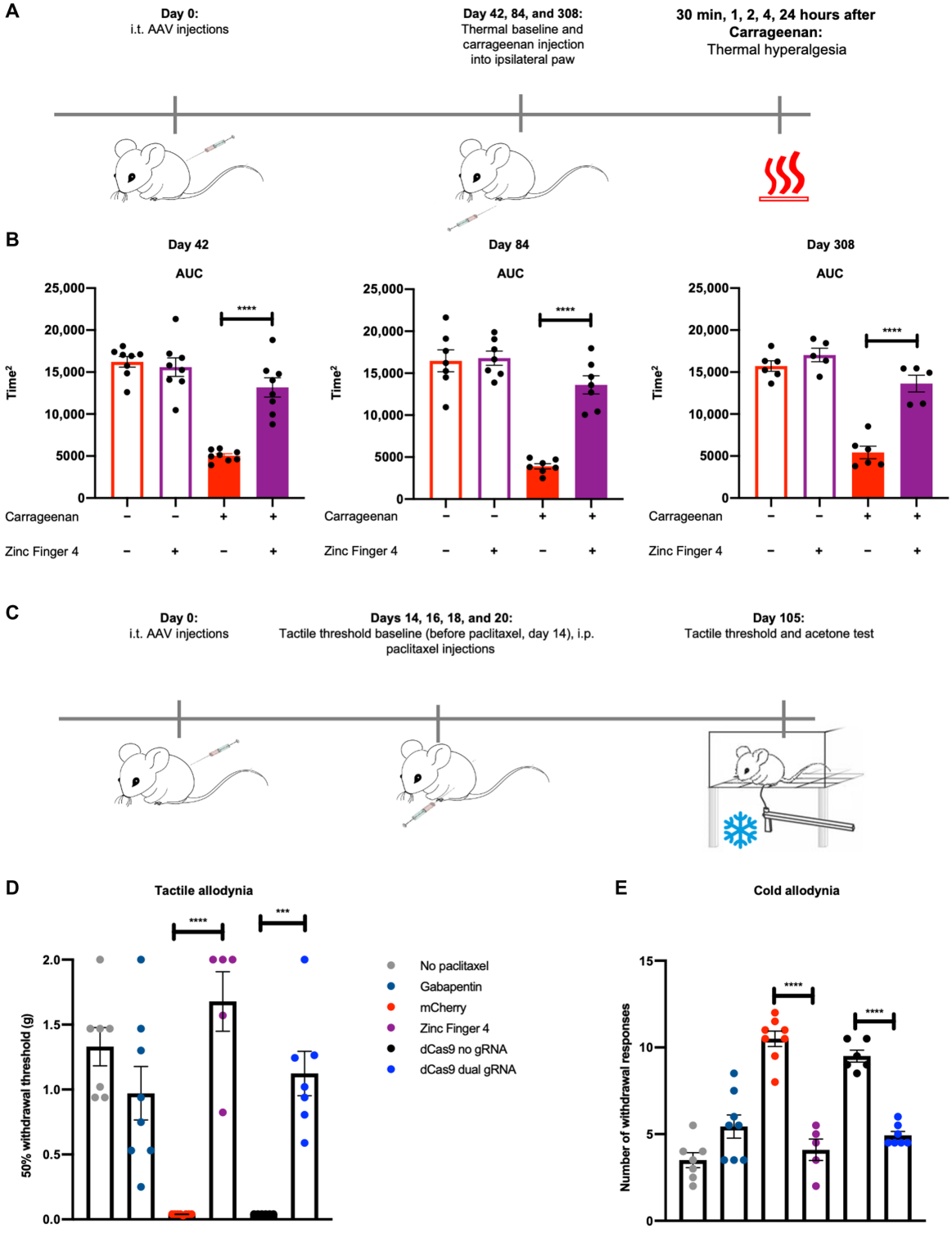

Fig. 6. Long-term efficacy of ZFP-KRAB and KRAB-dCas9 in two independent pain models. (**A**) Timeline of the carrageenan-induced inflammatory pain model. (**B**) The AUC of the aggregate PWL was calculated for both carrageenan- and saline-injected paws of mice 42, 84, and 308 days after intrathecal injection with AAV9-mCherry and AAV9-Zinc-Finger-4-KRAB. A significant increase in PWL is seen in the carrageenan-injected paws of mice injected with AAV9-Zinc-Finger-4-KRAB (dots represent individual biological replicates; $n = 5$ to 8; error bars are SEM; Student's t test, $^{****}P < 0.0001$). (**C**) Schematic of the paclitaxel-induced neuropathic pain model. (**D**) In situ repression of $Na_V1.7$ via Zinc-Finger-4-KRAB and KRAB-dCas9-dual-gRNA reduces paclitaxel-induced tactile allodynia 105 days after last paclitaxel injection (dots represent individual biological replicates; $n = 5$ to 8; error bars are SEM; Student's t test, $^{****}P < 0.0001$ and $^{***}P = 0.0001$). (**E**) In situ repression of $Na_V1.7$ via Zinc-Finger-4-KRAB and KRAB-dCas9-dual-gRNA reduces paclitaxel-induced cold allodynia (dots represent individual biological replicates; $n = 5$ to 8; error bars are SEM; Student's t test, $^{****}P < 0.0001$).

inclusions of unknown significance, and although they did not resemble known viral inclusions, these could not be ruled out and were scored. Possible mild edema of nerve (versus tissue processing artifact) was identified by some reviewers and was also graded. All reviewers reported some degree of mild focal inflammatory cell presence in some specimens, ranging from mast cells in nerve to lymphocytes in ganglia. No acute inflammation (neutrophils) was observed (fig. S5B). In summary, in all cases, the DRGs showed no loss of neurons, and the nerves showed no axonal injury or myelin pathology.

Last, we investigated the genome-wide effects of zinc finger– and CRISPR-mediated gene silencing on transcriptional regulation. For this, we performed whole-transcriptome RNA sequencing on Neuro2a cells transfected with either Zinc-Finger-4-KRAB and mCherry, or KRAB-dCas9-dual-gRNA and KRAB-dCas9-no-gRNA. We confirmed robust $Na_V1.7$ repression in both the Zinc-Finger-4-KRAB and KRAB-dCas9-dual-gRNA conditions (fig. S6, A and B). Overall, the KRAB-dCas9-dual-gRNA condition resulted in fewer off-target transcriptomic perturbations than the Zinc-Finger-4-KRAB construct. Next, to determine whether Zinc-Finger-4-KRAB and KRAB-dCas9-dual-gRNA were specific in vivo in DRGs in repressing only $Na_V1.7$ and not other expressed Na_V channels that are implicated in nociceptive transmission and/or that contribute to the hyperexcitability in primary afferent nociceptive and sympathetic neurons, the expression of $Na_V1.3$, $Na_V1.7$, $Na_V1.8$, and $Na_V1.9$ was determined by qPCR (fig. S6, C and D) of mice lumbar DRG from the post-chronic pain model ($n = 6$; Fig. 3, B and C). We observed significant repression of $Na_V1.7$, but not of $Na_V1.3$, $Na_V1.8$, or $Na_V1.9$, in mice injected with AAV9-Zinc-Finger-4-KRAB ($P < 0.0001$) and AAV9-KRAB-dCas9-dual-gRNA ($P = 0.0092$) (fig. S6, C and D). Together, we confirmed that both the CRISPR and zinc finger approaches for targeted gene regulation were highly specific.

Reduced excitability of DRG neurons

Last, using microelectrode array (MEA) recordings, we examined the impact of $Na_V1.7$ repression on excitability of DRG neurons transduced with AAV9-Zinc-Finger-4 in response to noxious heat. We tested firing from DRG neurons transduced in cell culture with either AAV9-mCherry or AAV9-Zinc-Finger-4 at both 37° and 42°C. We observed that both groups had increased firing when the temperature was raised, and the AAV9-mCherry group had more active electrodes per well as compared to the AAV9-Zinc-Finger-4 group at 37°C ($P = 0.0248$) (fig. S7).

DISCUSSION

In this study, we investigated the efficacy of the repression of $Na_V1.7$ in the DRG using two distinct epigenome engineering platforms—KRAB-dCas9 and ZFP-KRAB proteins—to prevent and treat acute and persistent nociceptive processing generated in murine models of peripheral inflammation and polyneuropathy. We believe that the promising results reflecting efficacy, tolerability, and absence of adverse events suggest the utility of the approach for developing therapeutic reagents.

Specifically, we found that mice injected with either epigenetic platform (ZFP-KRAB and KRAB-dCas9) had reduced expression of $Na_V1.7$ in DRG. Other studies have shown that partial repression of $Na_V1.7$ is sufficient to ameliorate pain (*43*–*47*). Using antisense oligonucleotides, mechanical pain could be ameliorated with 30 to 80% $Na_V1.7$ repression levels (*43*). Using microRNA-30b, around 50% repression of $Na_V1.7$ relieved neuropathic pain (*44*), whereas more recently microRNA-182 ameliorated pain preventing $Na_V1.7$ overexpression in spared nerve injury rats (*45*). Similarly, short hairpin RNA (shRNA)–mediated knockdown of $Na_V1.7$ prevented its overexpression in burn injury relieving pain (*46*). In addition, shRNA lentiviral vectors can reduce bone cancer pain by repressing $Na_V1.7$ 40 to 60% (*47*). Further studies are needed to determine what the minimum dosage to have an effect is.

The role of $Na_V1.7$ has been implicated in a variety of preclinical models, including those associated with robust inflammation as in the rodent carrageenan and complete Freund's adjuvant (CFA) model. Our studies demonstrate that $Na_V1.7$ knockdown via either epigenetic platform leads to reduced hypersensitivity to heat in a carrageenan inflammatory pain model. Similar results were obtained with a $Na_V1.7$ conditional knockout mice—$Na_V1.7$ is deleted from sensory neurons that express $Na_V1.8$—using a CFA model of inflammatory pain (*48*). This indicates an essential contribution of $Na_V1.7$ to hypersensitivity to heat stimuli after inflammation. We also examined the effect of knocking down $Na_V1.7$ in a paclitaxel-induced polyneuropathy. Previous work has shown that this treatment will induce $Na_V1.7$ (*33*). Both epigenetic repressors ameliorate tactile allodynia to a greater extent as the internal comparator gabapentin and were efficacious pre-emptively (before the pain state), as well as after the stabilization of a polyneuropathic chronic pain state. Last, we further addressed the role of $Na_V1.7$ knockdown in hyperpathia induced by intrathecal injection of BzATP. This was attenuated in mice previously treated with KRAB-dCas9. Spinal purine receptors have been shown to play a pivotal role in the nociceptive processing initiated by a variety of stimulus conditions including inflammatory/incisional pain and a variety of neuropathies (*49*). The present observations suggest that the repression of afferent $Na_V1.7$ expression in the nociceptor leads to a suppression of enhanced tactile sensitivity induced centrally. The mechanism underlying these results may reflect upon the observation that down-regulation of $Na_V1.7$ in the afferent may serve to minimize the activation of microglia and astrocytes (*47*). These results suggest that, at least partially, pain signal transduction through $Na_V1.7$ is downstream of ATP signaling.

Of note, the effects examined in the polyneuropathy and carrageenan model appeared to persist unchanged for at least 15 and 44 weeks for the paclitaxel-induced polyneuropathy and carrageenan models, respectively. Long-term expression has been similarly noted in other gene therapy studies (*50*, *51*). These effects were unaccompanied by any detectable adverse motor, olfactory, and neurological effects after neuraxial down-regulation of $Na_V1.7$.

We also confirmed the specificity of ZFP-KRAB and KRAB-dCas9 repression, via RNA sequencing of Neuro2a-transfected cells, with the latter approach being more specific for the reagents tested in this study. Toward the former, future structure-guided engineering of the zinc finger backbone could be explored to reduce off-target binding while maintaining on-target activity (*52*, *53*).

As other Na_V channels are implicated in nociceptive transmission and/or contribute to the hyperexcitability in primary afferent nociceptive and sympathetic neurons, the epigenetic engineering platforms presented in this study could be potentially applied to target these channels alone or in combination as potential therapeutics for pain. Previous studies demonstrated that intrathecal delivery of shRNA to knockdown $Na_V1.3$ attenuated nerve injury–induced pain and tactile allodynia in STZ-induced diabetic rats (*54*, *55*). In addition, mechanical and thermal allodynia were ameliorated after

peripheral inflammation and nerve injury, in a model of bone cancer pain with intrathecal delivery of antisense oligodeoxynucleotides (ASOs) or small interfering RNA (siRNA) targeting $Na_V1.8$ (*56*, *57*), and in a model of bone cancer pain with intrathecal delivery of ASOs targeting $Na_V1.9$ (*58*).

The intrathecal route of delivery represents an appropriate choice for this therapeutic approach. The role played by $Na_V1.7$ is in the nociceptive afferents, and their cell bodies are in the respective segmental DRG neurons. The intrathecal delivery route, as compared to systemic delivery, efficiently delivers AAVs to the DRG neurons that minimizes the possibility of off-target biodistribution and reduces the viral load required to get transduction. Although lumbar AAV intrathecal injections do not evade vector escape to the peripheral organs (*59*), studies in nonhuman primates (NHPs) demonstrated a highly reduced peripheral biodistribution and higher DRG transduction efficacy when AAV9 was injected as a lumbar intrathecal injection as compared to intravenously (*60*). At the very least, this reflects the lower total viral load required after spinal versus systemic delivery for a neuraxial target. Further, the relative paucity of B and T cells in the cerebrospinal fluid also serves to minimize the potential immune response. In one study, the presence of circulating anti-AAV neutralizing antibodies of up to a 1:128 titer had no inhibitory effect on the transduction efficacy in the central nervous system (CNS) after AAV9 intrathecal delivery in NHP (*60*). In addition, the extent of liver transduction after AAV9 intrathecal lumbar puncture was dependent on the presence of preexisting neutralizing antibodies against AAV9 but had no impact on CNS transduction (*60*, *61*). The transgene can also provoke an immunological response, and as ZFPs are engineered on human protein chassis, they intrinsically constitute a targeting approach with even lower potential immunogenicity. A study in NHPs found that intrathecal delivery of a non–self-protein (AAV9–green fluorescent protein) produced immune responses that were not seen with the delivery of a self-protein (*62*).

As a potential clinical treatment, KRAB-dCas9 and ZFP-KRAB show promise for treating chronic inflammatory and neuropathic pain. These systems allow for transient gene therapy, which is advantageous in the framework of chronic pain, because permanent pain insensitivity is not desired. Although the treatment is transient, the long duration still presents a substantial advantage compared to existing drugs, which must be taken daily or hourly, and which may have undesirable addictive effects. The use of multiple neuraxial interventions over time is a common motif for clinical interventions as with epidural steroids where repeat epidural delivery may occur over the year at several month intervals (*63*). It should be noted that this therapeutic regimen addresses a critical pain phenotype: the enduring but reversible pain state. Chronic pain defined as pain states enduring greater than 3 months are not necessarily irreversible. Because of advances in medicine, the number of cancer survivors is steadily increasing in the last decades. This increase has led to a subsequent increase in the number of cancer-related side effects, and chemotherapy-induced polyneuropathy is one of the most common adverse events (*64*).

These results displaying target engagement and efficacy provide strong support for the development of these platforms for pain control. Several limitations are pertinent. Although this study shows promise in treating acute and persistent nociceptive processing in the mouse model, species differences in $Na_V1.7$ expression (*33*, *65*) could mean that a different amount of repression might be needed for a phenotypic improvement in the human setting, as the expression of $Na_V1.7$ is higher in human DRG than in mice DRG. In addition, quantifying changes in $Na_V1.7$ protein could strengthen the study; however, five different antibodies were tested without any success (ab65167, ab85015, GTX134494, ASC-008, and AGP-057). Other researchers have also experienced the difficulty of measuring protein with $Na_V1.7$ antibodies. A recent paper (*66*) tried five different $Na_V1.7$ antibodies to stain mice DRG without any success and instead used an enzyme-linked immunosorbent assay (E03N0034); however, this kit is no longer commercially available. In addition, in another study (*67*), researchers used CRISPR to introduce a hemagglutinin (HA) tag to $Na_V1.7$ to be able to detect protein quantities. Because of its long-lasting effect, this therapy would be better suited for chronic conditions, and hence, modifications in delivery approach or addition of an inducible system might allow this approach to be used for acute pain conditions as well. In addition, further studies will be necessary to (i) determine what is the minimum effective AAV dosage to produce knockdown and therapeutic effects. (ii) Although long-term studies were performed (308 days after a single intrathecal injection), studies to evaluate the actual duration of treatment and whether any compensatory mechanisms take place because of $Na_V1.7$ repression must be performed. In particular, previous work has reported compensatory changes in the endogenous opioid system (proenkephalin up-regulation) in response to $Na_V1.7$ knockout in mice (*68*–*70*). (iii) Further studies must be performed to explore the properties of repeat dosing at the spinal level. (iv) Overall, we validated our approach in three mouse pain models. However, other models of inflammatory pain should be tested to further validate our results. (v) Last, other species including NHPs must be explored to further validate this approach and to determine potential toxicity and specificity before its translation into the clinic. Together, the results of these studies, albeit a proof of concept, show a promising new avenue for treatment of chronic pain, an important and increasingly urgent issue in our society.

MATERIALS AND METHODS

Study design

This study aimed to use two distinct epigenome engineering platforms—KRAB-dCas9 and ZF-KRAB proteins—for targeted $Na_V1.7$ repression in the DRG to prevent and treat acute and persistent nociceptive processing generated in murine models of peripheral inflammation and polyneuropathy, resulting in reduction of $Na_V1.7$ RNA transcripts and a decrease in carrageenan-induced thermal hyperalgesia, in paclitaxel-induced mechanical and cold hyperalgesia, and in BzATP-induced mechanical hyperalgesia. We identified gRNAs and ZFPs that repress $Na_V1.7$ in cultured cells and in vivo. We used AAV to deliver both epigenome engineering platforms in vivo and evaluated $Na_V1.7$ repression using quantitative reverse transcription PCR, RNA sequencing, and in situ RNA–fluorescence in situ hybridization (FISH) and the phenotypic effects using models of carrageenan-induced inflammatory pain, paclitaxel-induced neuropathic pain, BzATP-induced pain, and electrophysiology using multielectrode arrays. Mice injected with either mCherry or KRAB-dCas9 with no gRNA served as controls. All the experimental samples were included in the analysis, with no data excluded. Mice were randomized into groups, with mice from different AAV-injected groups being present in the same cage. Investigators performing behavioral assays were blinded to the experimental conditions. Sample size was selected on the basis of previous studies

(*34*, *71*, *72*), and statistical significance using similar behavioral models and a power analysis was not performed.

Statistical analysis

Results are expressed as means ± SEM. Statistical analysis was performed using GraphPad Prism (version 8.0, GraphPad Software). Results were analyzed using Student's *t* test (for differences between two groups), one-way ANOVA (for multiple groups), or two-way ANOVA (for multiple-group time-course experiments). Differences between groups with $P < 0.05$ were considered statistically significant.

SUPPLEMENTARY MATERIALS

stm.sciencemag.org/cgi/content/full/13/584/eaay9056/DC1
Materials and Methods
Fig. S1. In vitro optimization of epigenetic genome engineering tools to enable $Na_V1.7$ repression.
Fig. S2. Quantification of DRG transduction efficiencies via AAVs and carrageenan-induced inflammation in mice.
Fig. S3. Benchmarking of in situ repression of $Na_V1.7$ using ZFP-KRAB with established small-molecule drug gabapentin.
Fig. S4. Examining the safety of in situ repression of $Na_V1.7$ via ZFP-KRAB and KRAB-dCas9.
Fig. S5. Neuropathology analyses of DRGs targeted via AAVs.
Fig. S6. Genome-wide analysis of gene expression in zinc finger or CRISPR-treated Neuro2a cells.
Fig. S7. Multielectrode array recordings of DRG neurons transduced with AAV9-Zinc-Finger-4 show reduced response to heat.
Table S1. CRISPR-Cas9 gRNA spacer sequences.
Table S2. ZFP genomic target sequences.
Table S3. qPCR primers.
References (*73*–*94*)

View/request a protocol for this paper from *Bio-protocol*.

REFERENCES AND NOTES

1. C. B. Johannes, T. K. Le, X. Zhou, J. A. Johnston, R. H. Dworkin, The prevalence of chronic pain in United States adults: Results of an internet-based survey. *J. Pain* **11**, 1230–1239 (2010).
2. H. Breivik, B. Collett, V. Ventafridda, R. Cohen, D. Gallacher, Survey of chronic pain in Europe: Prevalence, impact on daily life, and treatment. *Eur. J. Pain* **10**, 287–333 (2006).
3. K. M. Baumbauer, E. E. Young, A. R. Starkweather, J. W. Guite, B. S. Russell, R. C. Manworren, Managing chronic pain in special populations with emphasis on pediatric, geriatric, and drug abuser populations. *Med. Clin. North Am.* **100**, 183–197 (2016).
4. O. A. de Leon-Casasola, Opioids for chronic pain: New evidence, new strategies, safe prescribing. *Am. J. Med.* **126**, S3–S11 (2013).
5. T. Berta, Y. Qadri, P.-H. Tan, R.-R. Ji, Targeting dorsal root ganglia and primary sensory neurons for the treatment of chronic pain. *Expert Opin. Ther. Targets* **21**, 695–703 (2017).
6. S. R. Chaplan, F. W. Bach, S. L. Shafer, T. L. Yaksh, Prolonged alleviation of tactile allodynia by intravenous lidocaine in neuropathic rats. *Anesthesiology* **83**, 775–785 (1995).
7. M. S. Wallace, J. Lee, L. Sorkin, J. S. Dunn, T. Yaksh, A. Yu, Intravenous lidocaine: Effects on controlling pain after anti-GD2 antibody therapy in children with neuroblastoma—A report of a series. *Anesth. Analg.* **85**, 794–796 (1997).
8. J. J. Cox, F. Reimann, A. K. Nicholas, G. Thornton, E. Roberts, K. Springell, G. Karbani, H. Jafri, J. Mannan, Y. Raashid, L. Al-Gazali, H. Hamamy, E. M. Valente, S. Gorman, R. Williams, D. P. McHale, J. N. Wood, F. M. Gribble, C. G. Woods, An SCN9A channelopathy causes congenital inability to experience pain. *Nature* **444**, 894–898 (2006).
9. C. Han, J. Huang, S. G. Waxman, Sodium channel Nav1.8: Emerging links to human disease. *Neurology* **86**, 473–483 (2016).
10. R. Castoro, M. Simmons, V. Ravi, D. Huang, C. Lee, J. Sergent, L. Zhou, J. Li, *SCN11A* Arg225Cys mutation causes nociceptive pain without detectable peripheral nerve pathology. *Neurol. Genet.* **4**, e255 (2018).
11. D. L. H. Bennett, C. G. Woods, Painful and painless channelopathies. *Lancet Neurol.* **13**, 587–599 (2014).
12. Y. Yang, M. A. Mis, M. Estacion, S. D. Dib-Hajj, S. G. Waxman, $Na_V1.7$ as a pharmacogenomic target for pain: Moving toward precision medicine. *Trends Pharmacol. Sci.* **39**, 258–275 (2018).
13. S. D. Dib-Hajj, Y. Yang, J. A. Black, S. G. Waxman, The $Na_V1.7$ sodium channel: From molecule to man. *Nat. Rev. Neurosci.* **14**, 49–62 (2013).
14. K. Kingwell, Nav1.7 withholds its pain potential. *Nat. Rev. Drug Discov.* **18**, 321–323 (2019).
15. C. J. Hutchings, P. Colussi, T. G. Clark, Ion channels as therapeutic antibody targets. *MAbs* **11**, 265–296 (2019).
16. F. Reimann, J. J. Cox, I. Belfer, L. Diatchenko, D. V. Zaykin, D. P. McHale, J. P. H. Drenth, F. Dai, J. Wheeler, F. Sanders, L. Wood, T.-X. Wu, J. Karppinen, L. Nikolajsen, M. Mannikko, M. B. Max, C. Kiselycznyk, M. Poddar, R. H. M. Te Morsche, S. Smith, D. Gibson, A. Kelempisioti, W. Maixner, F. M. Gribble, C. G. Woods, Pain perception is altered by a nucleotide polymorphism in SCN9A. *Proc. Natl. Acad. Sci. U.S.A.* **107**, 5148–5153 (2010).
17. M. Calvo, A. J. Davies, H. L. Hébert, G. A. Weir, E. J. Chesler, N. B. Finnerup, R. C. Levitt, B. H. Smith, G. G. Neely, M. Costigan, D. L. Bennett, The genetics of neuropathic pain from model organisms to clinical application. *Neuron* **104**, 637–653 (2019).
18. Q. Xu, B. Chou, B. Fitzsimmons, A. Miyanohara, V. Shubayev, C. Santucci, M. Hefferan, M. Marsala, X.-Y. Hua, In vivo gene knockdown in rat dorsal root ganglia mediated by self-complementary adeno-associated virus serotype 5 following intrathecal delivery. *PLOS ONE* **7**, e32581 (2012).
19. L. Vulchanova, D. J. Schuster, L. R. Belur, M. S. Riedl, K. M. Podetz-Pedersen, K. F. Kitto, G. L. Wilcox, R. S. McIvor, C. A. Fairbanks, Differential adeno-associated virus mediated gene transfer to sensory neurons following intrathecal delivery by direct lumbar puncture. *Mol. Pain* **6**, 31 (2010).
20. N. Hardcastle, N. M. Boulis, T. Federici, AAV gene delivery to the spinal cord: Serotypes, methods, candidate diseases, and clinical trials. *Expert Opin. Biol. Ther.* **18**, 293–307 (2018).
21. A. Pickar-Oliver, C. A. Gersbach, The next generation of CRISPR-Cas technologies and applications. *Nat. Rev. Mol. Cell Biol.* **20**, 490–507 (2019).
22. L. A. Gilbert, M. A. Horlbeck, B. Adamson, J. E. Villalta, Y. Chen, E. H. Whitehead, C. Guimaraes, B. Panning, H. L. Ploegh, M. C. Bassik, L. S. Qi, M. Kampmann, J. S. Weissman, Genome-scale CRISPR-mediated control of gene repression and activation. *Cell* **159**, 647–661 (2014).
23. P. I. Thakore, A. M. D'Ippolito, L. Song, A. Safi, N. K. Shivakumar, A. M. Kabadi, T. E. Reddy, G. E. Crawford, C. A. Gersbach, Highly specific epigenome editing by CRISPR-Cas9 repressors for silencing of distal regulatory elements. *Nat. Methods* **12**, 1143–1149 (2015).
24. A. M. Moreno, X. Fu, J. Zhu, D. Katrekar, Y. R. V. Shih, J. Marlett, J. Cabotaje, J. Tat, J. Naughton, L. Lisowski, S. Varghese, K. Zhang, P. Mali, In situ gene therapy via AAV-CRISPR-Cas9-mediated targeted gene regulation. *Mol. Ther.* **26**, 1818–1827 (2018).
25. P. I. Thakore, J. B. Kwon, C. E. Nelson, D. C. Rouse, M. P. Gemberling, M. L. Oliver, C. A. Gersbach, RNA-guided transcriptional silencing in vivo with *S. aureus* CRISPR-Cas9 repressors. *Nat. Commun.* **9**, 1674 (2018).
26. A. Lupo, E. Cesaro, G. Montano, D. Zurlo, P. Izzo, P. Costanzo, KRAB-zinc finger proteins: A repressor family displaying multiple biological functions. *Curr. Genomics* **14**, 268–278 (2013).
27. Y. G. Kim, J. Cha, S. Chandrasegaran, Hybrid restriction enzymes: Zinc finger fusions to Fok I cleavage domain. *Proc. Natl. Acad. Sci. U.S.A.* **93**, 1156–1160 (1996).
28. R. R. Beerli, D. J. Segal, B. Dreier, C. F. Barbas III, Toward controlling gene expression at will: Specific regulation of the *erbB-2/HER-2* promoter by using polydactyl zinc finger proteins constructed from modular building blocks. *Proc. Natl. Acad. Sci. U.S.A.* **95**, 14628–14633 (1998).
29. H. J. Kim, H. J. Lee, H. Kim, S. W. Cho, J.-S. Kim, Targeted genome editing in human cells with zinc finger nucleases constructed via modular assembly. *Genome Res.* **19**, 1279–1288 (2009).
30. N. S. Gregory, A. L. Harris, C. R. Robinson, P. M. Dougherty, P. N. Fuchs, K. A. Sluka, An overview of animal models of pain: Disease models and outcome measures. *J. Pain* **14**, 1255–1269 (2013).
31. J. A. Black, S. Liu, M. Tanaka, T. R. Cummins, S. G. Waxman, Changes in the expression of tetrodotoxin-sensitive sodium channels within dorsal root ganglia neurons in inflammatory pain. *Pain* **108**, 237–247 (2004).
32. R. Radhakrishnan, S. A. Moore, K. A. Sluka, Unilateral carrageenan injection into muscle or joint induces chronic bilateral hyperalgesia in rats. *Pain* **104**, 567–577 (2003).
33. W. Chang, T. Berta, Y. H. Kim, S. Lee, S.-Y. Lee, R.-R. Ji, Expression and role of voltage-gated sodium channels in human dorsal root ganglion neurons with special focus on Nav1.7, species differences, and regulation by paclitaxel. *Neurosci. Bull.* **34**, 4–12 (2017).
34. W. Toma, S. L. Kyte, D. Bagdas, Y. Alkhlaif, S. D. Alsharari, A. H. Lichtman, Z.-J. Chen, E. Del Fabbro, J. W. Bigbee, D. A. Gewirtz, M. I. Damaj, Effects of paclitaxel on the development of neuropathy and affective behaviors in the mouse. *Neuropharmacology* **117**, 305–315 (2017).
35. A. I. Basbaum, D. M. Bautista, G. Scherrer, D. Julius, Cellular and molecular mechanisms of pain. *Cell* **139**, 267–284 (2009).
36. F. M. Munoz, R. Gao, Y. Tian, B. A. Henstenburg, J. E. Barrett, H. Hu, Neuronal P2X7 receptor-induced reactive oxygen species production contributes to nociceptive behavior in mice. *Sci. Rep.* **7**, 3539 (2017).
37. D. J. Schuster, J. A. Dykstra, M. S. Riedl, K. F. Kitto, L. R. Belur, R. S. McIvor, R. P. Elde, C. A. Fairbanks, L. Vulchanova, Biodistribution of adeno-associated virus serotype 9 (AAV9) vector after intrathecal and intravenous delivery in mouse. *Front. Neuroanat.* **8**, 42 (2014).

38. Y. Lu, K. N. Westlund, Gabapentin attenuates nociceptive behaviors in an acute arthritis model in rats. *J. Pharmacol. Exp. Ther.* **290**, 214–219 (1999).
39. C. K. Jones, S. C. Peters, H. E. Shannon, Efficacy of duloxetine, a potent and balanced serotonergic and noradrenergic reuptake inhibitor, in inflammatory and acute pain models in rodents. *J. Pharmacol. Exp. Ther.* **312**, 726–732 (2005).
40. R. J. Carter, J. Morton, S. B. Dunnett, Motor coordination and balance in rodents. *Curr. Protoc. Neurosci.* **15**, 8.12.1–8.12.14 (2001).
41. R. M. J. Deacon, Assessing nest building in mice. *Nat. Protoc.* **1**, 1117–1119 (2006).
42. J. Weiss, M. Pyrski, E. Jacobi, B. Bufe, V. Willnecker, B. Schick, P. Zizzari, S. J. Gossage, C. A. Greer, T. Leinders-Zufall, C. G. Woods, J. N. Wood, F. Zufall, Loss-of-function mutations in sodium channel Nav1.7 cause anosmia. *Nature* **472**, 186–190 (2011).
43. A. Mohan, B. Fitzsimmons, H. T. Zhao, Y. Jiang, C. Mazur, E. E. Swayze, H. B. Kordasiewicz, Antisense oligonucleotides selectively suppress target RNA in nociceptive neurons of the pain system and can ameliorate mechanical pain. *Pain* **159**, 139–149 (2018).
44. J. Shao, J. Cao, J. Wang, X. Ren, S. Su, M. Li, Z. Li, Q. Zhao, W. Zang, MicroRNA-30b regulates expression of the sodium channel Nav1.7 in nerve injury-induced neuropathic pain in the rat. *Mol. Pain* **12**, 1744806916671523 (2016).
45. W. Cai, Q. Zhao, J. Shao, J. Zhang, L. Li, X. Ren, S. Su, Q. Bai, M. Li, X. Chen, J. Wang, J. Cao, W. Zang, MicroRNA-182 alleviates neuropathic pain by regulating Nav1.7 following spared nerve injury in rats. *Sci. Rep.* **8**, 16750 (2018).
46. W. Cai, J. Cao, X. Ren, L. Qiao, X. Chen, M. Li, W. Zang, shRNA mediated knockdown of Nav1.7 in rat dorsal root ganglion attenuates pain following burn injury. *BMC Anesthesiol.* **16**, 59 (2016).
47. J. Pan, X.-J. Lin, Z.-H. Ling, Y.-Z. Cai, Effect of down-regulation of voltage-gated sodium channel Nav1.7 on activation of astrocytes and microglia in DRG in rats with cancer pain. *Asian Pac. J. Trop. Med.* **8**, 405–411 (2015).
48. S. D. Shields, X. Cheng, N. Uçeyler, C. Sommer, S. D. Dib-Hajj, S. G. Waxman, Sodium channel Nav1.7 is essential for lowering heat pain threshold after burn injury. *J. Neurosci.* **32**, 10819–10832 (2012).
49. L.-P. Bernier, A. R. Ase, P. Séguéla, P2X receptor channels in chronic pain pathways. *Br. J. Pharmacol.* **175**, 2219–2230 (2018).
50. M. Zahur, J. Tolö, M. Bahr, S. Kugler, Long-term assessment of AAV-mediated zinc finger nuclease expression in the mouse brain. *Front. Mol. Neurosci.* **10**, 142 (2017).
51. S. J. Aronson, R. S. Bakker, X. Shi, S. Duijst, L. Ten Bloemendaal, D. R. de Waart, J. Verheij, G. Ronzitti, R. P. Oude Elferink, U. Beuers, C. C. Paulusma, P. J. Bosma, Liver-directed gene therapy results in long-term correction of progressive familial intrahepatic cholestasis type 3 in mice. *J. Hepatol.* **71**, 153–162 (2019).
52. N. Dimitrova, J. R. Zamudio, R. M. Jong, D. Soukup, R. Resnick, K. Sarma, A. J. Ward, A. Raj, J. Lee, P. A. Sharp, T. Jacks, A synthetic biology framework for programming eukaryotic transcription functions. *Cell* , (2012).
53. J. C. Miller, D. P. Patil, D. F. Xia, C. B. Paine, F. Fauser, H. W. Richards, D. A. Shivak, Y. R. Bendaña, S. J. Hinkley, N. A. Scarlott, S. C. Lam, A. Reik, Y. Zhou, D. E. Paschon, P. Li, T. Wangzor, G. Lee, L. Zhang, E. J. Rebar, Enhancing gene editing specificity by attenuating DNA cleavage kinetics. *Nat. Biotechnol.* **37**, 945–952 (2019).
54. O. A. Samad, A. M. Tan, X. Cheng, E. Foster, S. D. Dib-Hajj, S. G. Waxman, Virus-mediated shRNA knockdown of Nav1.3 in rat dorsal root ganglion attenuates nerve injury-induced neuropathic pain. *Mol. Ther.* **21**, 49–56 (2013).
55. A. M. Tan, O. A. Samad, S. D. Dib-Hajj, S. G. Waxman, Virus-mediated knockdown of Nav1.3 in dorsal root ganglia of STZ-induced diabetic rats alleviates tactile allodynia. *Mol. Med.* **21**, 544–552 (2015).
56. S. K. Joshi, J. P. Mikusa, G. Hernandez, S. Baker, C. C. Shieh, T. Neelands, X. F. Zhang, W. Niforatos, K. Kage, P. Han, D. Krafte, C. Faltynek, J. P. Sullivan, M. F. Jarvis, P. Honore, Involvement of the TTX-resistant sodium channel Nav 1.8 in inflammatory and neuropathic, but not post-operative, pain states. *Pain* **123**, 75–82 (2006).
57. X. W. Dong, S. Goregoaker, H. Engler, X. Zhou, L. Mark, J. Crona, R. Terry, J. Hunter, T. Priestley, Small interfering RNA-mediated selective knockdown of NaV1.8 tetrodotoxin-resistant sodium channel reverses mechanical allodynia in neuropathic rats. *Neuroscience* **146**, 812–821 (2007).
58. F. Zhang, Y. Wang, Y. Liu, H. Han, D. Zhang, X. Fan, X. Du, N. Gamper, H. Zhang, Transcriptional regulation of voltage-gated sodium channels contributes to GM-CSF-induced pain. *J. Neurosci.* **39**, 5222–5233 (2019).
59. C. Hinderer, P. Bell, C. H. Vite, J. P. Louboutin, R. Grant, E. Bote, H. Yu, B. Pukenas, R. Hurst, J. M. Wilson, Widespread gene transfer in the central nervous system of cynomolgus macaques following delivery of AAV9 into the cisterna magna. *Mol. Ther. Methods Clin. Dev.* **1**, 14051 (2014).
60. S. J. Gray, S. Nagabhushan Kalburgi, T. J. McCown, R. Jude Samulski, Global CNS gene delivery and evasion of anti-AAV-neutralizing antibodies by intrathecal AAV administration in non-human primates. *Gene Ther.* **20**, 450–459 (2013).
61. V. Haurigot, S. Marcó, A. Ribera, M. Garcia, A. Ruzo, P. Villacampa, E. Ayuso, S. Añor, A. Andaluz, M. Pineda, G. García-Fructuoso, M. Molas, L. Maggioni, S. Muñoz, S. Motas, J. Ruberte, F. Mingozzi, M. Pumarola, F. Bosch, Whole body correction of mucopolysaccharidosis IIIA by intracerebrospinal fluid gene therapy. *J. Clin. Invest.* **123**, 3254–3271 (2013).
62. L. Samaranch, W. S. Sebastian, A. P. Kells, E. A. Salegio, G. Heller, J. R. Bringas, P. Pivirotto, S. DeArmond, J. Forsayeth, K. S. Bankiewicz, AAV9-mediated expression of a non-self protein in nonhuman primate central nervous system triggers widespread neuroinflammation driven by antigen-presenting cell transduction. *Mol. Ther.* **22**, 329–337 (2014).
63. L. Manchikanti, Y. Malla, K. A. Cash, V. Pampati, J. A. Hirsch, Comparison of effectiveness for fluoroscopic cervical interlaminar epidural injections with or without steroid in cervical post-surgery syndrome. *Korean J. Pain* **31**, 277–288 (2018).
64. N. P. Staff, A. Grisold, W. Grisold, A. J. Windebank, Chemotherapy-induced peripheral neuropathy: A current review. *Ann. Neurol.* **81**, 772–781 (2017).
65. T. C. Gonçalves, E. Benoit, M. Partiseti, D. Servent, The NaV1.7 channel subtype as an antinociceptive target for spider toxins in adult dorsal root ganglia neurons. *Front. Pharmacol.* **9**, 1000 (2018).
66. L. Hofmann, D. Hose, A. Grießhammer, R. Blum, F. Döring, S. Dib-Hajj, S. Waxman, C. Sommer, E. Wischmeyer, N. Üçeyler, Characterization of small fiber pathology in a mouse model of fabry disease. *eLife* **7**, e39300 (2018).
67. L. A. McDermott, G. A. Weir, A. C. Themistocleous, A. R. Segerdahl, I. Blesneac, G. Baskozos, A. J. Clark, V. Millar, L. J. Peck, D. Ebner, I. Tracey, J. Serra, D. L. Bennett, Defining the functional role of NaV1.7 in human nociception. *Neuron* **101**, 905–919.e8 (2019).
68. M. S. Minett, V. Pereira, S. Sikandar, A. Matsuyama, S. Lolignier, A. H. Kanellopoulos, F. Mancini, G. D. Iannetti, Y. D. Bogdanov, S. Santana-Varela, Q. Millet, G. Baskozos, R. MacAllister, J. J. Cox, J. Zhao, J. N. Wood, Endogenous opioids contribute to insensitivity to pain in humans and mice lacking sodium channel Nav1.7. *Nat. Commun.* **6**, 8967 (2015).
69. J. Isensee, L. Krahé, K. Moeller, V. Pereira, J. E. Sexton, X. Sun, E. Emery, J. N. Wood, T. Hucho, Synergistic regulation of serotonin and opioid signaling contributes to pain insensitivity in Nav1.7 knockout mice. *Sci. Signal.* **10**, eaah4874 (2017).
70. D. I. MacDonald, S. Sikandar, J. Weiss, M. Pyrski, A. P. Luiz, Q. Millet, E. C. Emery, F. Mancini, G. D. Iannetti, S. R. A. Alles, J. Zhao, J. J. Cox, R. M. Brownstone, F. Zufall, J. N. Wood, The mechanism of analgesia in $Na_V1.7$ null mutants. bioRxiv 2020.06.01.127183 [**Preprint**]. 2 June 2020. https://doi.org/10.1101/2020.06.01.127183.
71. S. J. Ward, M. D. Ramirez, H. Neelakantan, E. A. Walker, Cannabidiol prevents the development of cold and mechanical allodynia in paclitaxel-treated female C57Bl6 mice. *Anesth. Analg.* **113**, 947–950 (2011).
72. S. Sikandar, Y. Gustavsson, M. J. Marino, A. H. Dickenson, T. L. Yaksh, L. S. Sorkin, R. Ramachandran, Effects of intraplantar botulinum toxin-B on carrageenan-induced changes in nociception and spinal phosphorylation of GluA1 and Akt. *Eur. J. Neurosci.* **44**, 1714–1722 (2016).
73. M. A. Horlbeck, L. A. Gilbert, J. E. Villalta, B. Adamson, R. A. Pak, Y. Chen, A. P. Fields, C. Y. Park, J. E. Corn, M. Kampmann, J. S. Weissman, Compact and highly active next-generation libraries for CRISPR-mediated gene repression and activation. *eLife* **5**, e19760 (2016).
74. T. Yu, J. Zhu, Y. Li, Y. Ma, J. Wang, X. Cheng, S. Jin, Q. Sun, X. Li, H. Gong, Q. Luo, F. Xu, S. Zhao, D. Zhu, RTF: A rapid and versatile tissue optical clearing method. *Sci. Rep.* **8**, 1964 (2018).
75. K. Ichikizaki, S. Toya, T. Hoshino, A new procedure for lumbar puncture in the mouse (intrathecal injection) preliminary report. *Keio J. Med.* **28**, 165–171 (1979).
76. K. K. Lucas, C. I. Svensson, X.-Y. Hua, T. L. Yaksh, E. A. Dennis, Spinal phospholipase A2 in inflammatory hyperalgesia: Role of group IVA cPLA2. *Br. J. Pharmacol.* **144**, 940–952 (2005).
77. C. I. Svensson, K. K. Lucas, X.-Y. Hua, H. C. Powell, E. A. Dennis, T. L. Yaksh, Spinal phospholipase A2 in inflammatory hyperalgesia: Role of the small, secretory phospholipase A2. *Neuroscience* **133**, 543–553 (2005).
78. S. R. Chaplan, F. W. Bach, J. W. Pogrel, J. M. Chung, T. L. Yaksh, Quantitative assessment of tactile allodynia in the rat paw. *J. Neurosci. Methods* **53**, 55–63 (1994).
79. K. Hargreaves, R. Dubner, F. Brown, C. Flores, J. Joris, A new and sensitive method for measuring thermal nociception in cutaneous hyperalgesia. *Pain* **32**, 77–88 (1988).
80. J. Guindon, L. Deng, B. Fan, J. Wager-Miller, A. G. Hohmann, Optimization of a cisplatin model of chemotherapy-induced peripheral neuropathy in mice: Use of vitamin C and sodium bicarbonate pretreatments to reduce nephrotoxicity and improve animal health status. *Mol. Pain* **10**, 56 (2014).
81. A. Dobin, C. A. Davis, F. Schlesinger, J. Drenkow, C. Zaleski, S. Jha, P. Batut, M. Chaisson, T. R. Gingeras, STAR: Ultrafast universal RNA-seq aligner. *Bioinformatics* **29**, 15–21 (2013).
82. M. I. Love, W. Huber, S. Anders, Moderated estimation of fold change and dispersion for RNA-seq data with DESeq2. *Genome Biol.* **15**, 550 (2014).
83. D. A. Finn, A. J. Roberts, F. Lotrich, E. J. Gallaher, Genetic differences in behavioral sensitivity to a neuroactive steroid. *J. Pharmacol. Exp. Ther.* **280**, 820–828 (1997).
84. A. J. Roberts, E. J. Gallaher, L. D. Keith, Dissociation of the effect of aminoglutethimide on corticosterone biosynthesis from ataxic and hypothermic effects in DBA and C57 mice. *Neuroendocrinology* **58**, 303–309 (1993).

85. K. Njung'e, S. L. Handley, Evaluation of marble-burying behavior as a model of anxiety. *Pharmacol. Biochem. Behav.* **38**, 63–67 (1991).
86. A. Thomas, A. Burant, N. Bui, D. Graham, L. A. Yuva-Paylor, R. Paylor, Marble burying reflects a repetitive and perseverative behavior more than novelty-induced anxiety. *Psychopharmacology* **204**, 361–373 (2009).
87. F. S. S. Sousa, P. T. Birmann, R. Balaguez, D. Alves, C. A. Brüning, L. Savegnago, α-(phenylselanyl) acetophenone abolishes acute restraint stress induced-comorbid pain, depression and anxiety-related behaviors in mice. *Neurochem. Int.* **120**, 112–120 (2018).
88. E. Palazzo, R. Romano, L. Luongo, S. Boccella, D. De Gregorio, M. E. Giordano, F. Rossi, I. Marabese, M. A. Scafuro, V. De Novellis, S. Maione, MMPIP, an mGluR7-selective negative allosteric modulator, alleviates pain and normalizes affective and cognitive behavior in neuropathic mice. *Pain* **156**, 1060–1073 (2015).
89. D. G. Mumby, A. Tremblay, V. Lecluse, H. Lehmann, Hippocampal damage and anterograde object-recognition in rats after long retention intervals. *Hippocampus* **15**, 1050–1056 (2005).
90. B. D. Winters, S. E. Forwood, R. A. Cowell, L. M. Saksida, T. J. Bussey, Double dissociation between the effects of peri-postrhinal cortex and hippocampal lesions on tests of object recognition and spatial memory: Heterogeneity of function within the temporal lobe. *J. Neurosci.* **24**, 5901–5908 (2004).
91. C. K. J. Lieben, H. W. M. Steinbusch, A. Blokland, 5,7-DHT lesion of the dorsal raphe nuclei impairs object recognition but not affective behavior and corticosterone response to stressor in the rat. *Behav. Brain Res.* **168**, 197–207 (2006).
92. D. E. Berlyne, Stimulus intensity and attention in relation to learning theory. *Q. J. Exp. Psychol.* **2**, 71–75 (1950).
93. A. Ennaceur, J. Delacour, A new one-trial test for neurobiological studies of memory in rats. 1: Behavioral data. *Behav. Brain Res.* **31**, 47–59 (1988).
94. C. J. Heyser, A. Chemero, Novel object exploration in mice: Not all objects are created equal. *Behav. Processes* **89**, 232–238 (2012).

Acknowledgments: We thank members of the Mali and Yaksh laboratories for advice and help with experiments, D. Pizzo for help with the H&E staining, and the Salk GT3 viral core for help with AAV production. **Funding:** This work was supported by the University of California San Diego (UCSD) Institutional Funds and NIH grants (R01HG009285 to P.M., RO1CA222826 to P.M., RO1GM123313 to P.M., R43CA239940 to A.M.M. and F.A., R43NS112088 to A.M.M. and F.A., R01NS102432 to T.L.Y., and R01NS099338 to T.L.Y.) and NINDS NS47101 to the UCSD Microscopy Core. This publication includes data generated at the UCSD IGM Genomics Center using an Illumina NovaSeq 6000 that was purchased with funding from an NIH SIG grant (#S10 OD026929). A.M.M. acknowledges graduate fellowships from CONACYT and UCMEXUS. G.F.C. thanks FAPESP (grant 2018/05778-3). **Author contributions:** A.M.M. conceived and performed experiments, analyzed data, and wrote the manuscript. F.A. performed experiments, analyzed data, and wrote the manuscript. G.F.C. performed the BzATP experiments. M. Hunt and D.M. performed whole-DRG mount experiments and RNA-FISH. S.A.W. helped set up and design experiments. A.D. performed MEA experiments. A.P., M. Hu, L.D., and G.G.d.S. performed experiments. N.P. and U.P. performed RNA sequencing analyses. A.J.R. performed and analyzed animal safety studies. V.G., I.D., and R.F.H. performed histopathology analyses. T.L.Y. conceived and supervised the project, designed experiments, and wrote the manuscript. P.M. conceived and supervised the project, designed experiments, performed experiments, and wrote the manuscript. This article was prepared while S.A.W. was employed at the USCD. The opinions expressed in this article are the authors' own and do not reflect the views of the NIH, the Department of Health and Human Services, or the U.S. government. **Competing interests:** A.M.M. and P.M. have filed patents based on this work (CRISPR-Cas genome engineering via a modular AAV system, PCT/US2017/047687, and Long-lasting analgesia via targeted in vivo epigenetic repression, PCT/US2020/027541). A.M.M. and F.A. are cofounders and current employees of Navega Therapeutics. T.L.Y. is a member of the scientific advisory board for Navega Therapeutics. P.M. is a scientific cofounder of Shape Therapeutics, Boundless Biosciences, Seven Therapeutics, Navega Therapeutics, and Engine Biosciences. The terms of these arrangements have been reviewed and approved by the USCD in accordance with its conflict of interest policies. **Data and materials availability:** All data associated with this study are present in the paper or the Supplementary Materials.

Submitted 28 July 2019
Resubmitted 14 August 2020
Accepted 10 November 2020
Published 10 March 2021
10.1126/scitranslmed.aay9056

Citation: A. M. Moreno, F. Alemán, G. F. Catroli, M. Hunt, M. Hu, A. Dailamy, A. Pla, S. A. Woller, N. Palmer, U. Parekh, D. McDonald, A. J. Roberts, V. Goodwill, I. Dryden, R. F. Hevner, L. Delay, G. Gonçalves dos Santos, T. L. Yaksh, P. Mali, Long-lasting analgesia via targeted in situ repression of $Na_V1.7$ in mice. *Sci. Transl. Med.* **13**, eaay9056 (2021).

Science Translational Medicine

Long-lasting analgesia via targeted in situ repression of $Na_V1.7$ in mice

Ana M. Moreno, Fernando Alemán, Glaucilene F. Catroli, Matthew Hunt, Michael Hu, Amir Dailamy, Andrew Pla, Sarah A. Woller, Nathan Palmer, Udit Parekh, Daniella McDonald, Amanda J. Roberts, Vanessa Goodwill, Ian Dryden, Robert F. Hevner, Lauriane Delay, Gilson Gonçalves dos Santos, Tony L. Yaksh and Prashant Mali

Sci Transl Med **13**, eaay9056.
DOI: 10.1126/scitranslmed.aay9056

Repressing pain LATER

Opioids are the current standard of care for the treatment of chronic pain. However, they have severe side effects. Recent data have shown that loss-of-function mutations in the sodium channel $Na_V1.7$ cause insensitivity to pain. Here, Moreno *et al.* developed an epigenetic strategy using CRISPR-dCas9 and zinc fingers called long-lasting analgesia via targeted in vivo epigenetic repression of $Na_V1.7$ (LATER) to repress $Na_V1.7$. In vivo, LATER reduced hyperalgesia in multiple animal models and reversed chemotherapy-induced chronic pain in mice. The results suggest that LATER might be effective for treating chronic pain of multiple origins.

Science Translational Medicine
AAAS

stm.sciencemag.org/cgi/content/full/13/584/eaay9056/DC1

Supplementary Materials for

Long-lasting analgesia via targeted in situ repression of $Na_V1.7$ in mice

Ana M. Moreno, Fernando Alemán, Glaucilene F. Catroli, Matthew Hunt, Michael Hu, Amir Dailamy, Andrew Pla, Sarah A. Woller, Nathan Palmer, Udit Parekh, Daniella McDonald, Amanda J. Roberts, Vanessa Goodwill, Ian Dryden, Robert F. Hevner, Lauriane Delay, Gilson Gonçalves dos Santos, Tony L. Yaksh*, Prashant Mali*

*Corresponding author. Email: pmali@ucsd.edu (P.M.); tyaksh@ucsd.edu (T.L.Y.)

Published 10 March 2021, *Sci. Transl. Med.* **13**, eaay9056 (2021)
DOI: 10.1126/scitranslmed.aay9056

This PDF file includes:

MATERIALS AND METHODS

Vector Design and Construction

dCas9 and Zinc-Finger AAV vectors were constructed by sequential assembly of corresponding gene blocks (Integrated DNA Technologies) into a custom synthesized rAAV2 vector backbone. gRNA sequences were inserted into dNCas9 plasmids by cloning oligonucleotides (IDT) encoding spacers into AgeI cloning sites via Gibson assembly. gRNAs were designed utilizing an in silico tool to predict gRNAs *(73)*. For in vivo KRAB-dCas9 experiments, a dual-gRNA design was used (guides SCN9A-1 and SCN9A-2), except for the paclitaxel-induced neuropathic pain model in **Fig. 5**, which only utilized a single-gRNA (gRNA 2). ZF computational designs were obtained via Sigma.

Mammalian Cell Culture

Neuro2a cells were grown in EMEM supplemented with 10% fetal bovine serum (FBS) and 1% Antibiotic-Antimycotic (Thermo Fisher Scientific) in an incubator at 37°C and 5% CO_2 atmosphere.

Lipid-Mediated Cell Transfections

One day prior to transfection, Neuro2a cells were seeded in a 24-well plate at a cell density of 1 or 2 × 10^5 cells per well. 0.5 µg of each plasmid was added to 25 µL of Opti-MEM medium, followed by addition of 25 µL of Opti-MEM containing 2 µL of Lipofectamine 2000. The mixture was incubated at room temperature for 15 min. The entire solution was then added to the cells in a 24-well plate and mixed by gently swirling the plate. Media was changed after 24 h, and the plate was incubated at 37°C for 72 h in a 5% CO_2 incubator. Cells were harvested, spun down, and frozen at 80°C.

Production of AAVs

Virus was prepared by the Gene Transfer, Targeting and Therapeutics (GT3) core at the Salk Institute of Biological Studies (La Jolla, CA) or in-house utilizing the GT3 core protocol. Briefly, AAV2/9 virus particles were produced using HEK293T cells via the triple transfection method and purified via an iodixanol gradient. Confluency at transfection was between 80% and 90%. Media was replaced with pre-warmed media

2h before transfection. Each virus was produced in five 15 cm plates, where each plate was transfected with 10 µg of pXR-capsid (pXR-9), 10 of µg recombinant transfer vector, and 10 µg of pHelper vector using polyethylenimine (PEI; 1 mg/mL linear PEI in DPBS [pH 4.5], using HCl) at a PEI:DNA mass ratio of 4:1. The mixture was incubated for 10 min at room temperature and then applied dropwise onto the media. The virus was harvested after 72 h and purified using an iodixanol density gradient ultracentrifugation method. The virus was then dialyzed with 1x PBS (pH 7.2) supplemented with 50 mM NaCl and 0.0001% of Pluronic F68 (Thermo Fisher Scientific) using 50-kDa filters (Millipore) to a final volume of ~100 µL and quantified by qPCR using primers specific to the ITR region, against a standard (ATCC VR-1616): AAV-ITR-F: 5' -CGGCCTCAGTGAGCGA-3' and AAV-ITR-R: 5' -GGAACCCCTAGTGATGGAGTT-3'

Whole-DRG mounts

21 Days following i.t. injections of AAV9-mCherry, mice were transcardially perfused with 4% PFA and post-fixed in 4% PFA for 24 hours, then stored in PBS with 0.02% sodium azide. DRGs from cervical, thoracic, lumbar and sacral were dissected out and immediately cleared following the previously described RTF method *(74)*. In brief DRGs were immediately placed in a solution of 30% triethanolamine (TEA), 40% formamide, (F) and 30% nanopore water (H_20), for 15 minutes at room temperature on a shake plate, then transferred to a solution of 60% TEA, 25% F, and 15% H_20 for 15 minutes at room temperature on a shake plate, and finally transferred to a final solution of 70% TEA, 15% F, and 15% H_20 for 15-20 minutes (until clear). DRGs were then transferred into imaging chambers mounted on glass microscope slides. Imaging chambers were designed in house to be 400 µm high and fit 22 x 30 mm coverslips with a leakproof seal. Chambers were 3D printed using 3D resyn CR UHT, ApplyLabWork Tan, or polypropylene. Native mCherry expressing DRGs were then imaged on an inverted Leica TCS SP5 Confocal microscope at 10x to view the entire DRG or 63x for high resolution images. Images were analyzed using Imaris (bitplane) and ImageJ. Individual mCherry positive neurons were converted into 3D meshes within Imaris and quantified for volume and raw pixel intensity values. Data was analyzed in Prism and SPSS.

Animal Experiments

All animal procedures were performed in accordance with protocols approved by the Institutional Animal Care and Use Committee (IACUC) of the University of California,

San Diego. All mice were acquired from Jackson Laboratory. Two-month-old adult male C57BL/6J mice (25-30g) were housed with food and water provided *ad libitum*, under a 12 h light/dark cycle with up to 5 mice per cage. All behavioral tests were performed during the light cycle period.

Intrathecal AAV Injections

Anesthesia was induced with 2.5% isoflurane delivered in equal parts O_2 and room air in a closed chamber until a loss of the righting reflex was observed. The lower back of mice was shaven and swabbed with 70% ethanol. Mice were then intrathecally (i.t.) injected using a Hamilton syringe and 30G needle as previously described *(75)* between vertebrae L4 and L5 with 5 µL of AAV for a total of 1×10^{12} vg/mouse, unless otherwise noted in the manuscript. All CRISPR-dCas9 experiments received 1×10^{12} vg/mouse for each split-dCas9 AAV. A tail flick was considered indicative of appropriate needle placement. Following injection, all mice resumed motor activity consistent with that observed prior to i.t. injection.

Pain Models

Intraplantar carrageenan injection: Carrageenan-induced inflammation is a classic model of edema formation and hyperalgesia *(76–78)*. 21 days after AAV pre-treatment, anesthesia was induced as described above. Lambda carrageenan (Sigma Aldrich; 2% (W/V) dissolved in 0.9% (W/V) NaCl solution, 20 µL) was subcutaneously injected with a 30G needle into the plantar (ventral) surface of the ipsilateral paw. An equal amount of isotonic saline was injected into the contralateral paw. Paw thickness was measured with a caliper before and 4h after carrageenan/saline injections as an index of edema/inflammation. Hargreaves testing was performed before injection (t=0) and (t= 30, 60, 120, 240 minutes and 24 hours post-injection). The experimenter was blinded to the composition of treatment groups. Mice were euthanized after the 24-hour time point.

Paclitaxel-induced neuropathy: Paclitaxel (Tocris Biosciences, 1097) was dissolved in a mixture of 1:1:18 [1 volume ethanol/1 volume Cremophor EL (Millipore, 238470)/18 volumes of sterilized 0.9% (W/V) NaCl solution]. Paclitaxel injections (8 mg/kg) were administered intraperitoneally (i.p.) in a volume of 1 mL/100 g body weight every other day for a total of four injections to induce neuropathy (32 mg/kg), resulting in a cumulative human equivalent dose of 28.4–113.5 mg/m^2 as previously described *(34)*. Behavioral tests were performed 24 hours or 105 days after the last dosage for mice that

were pretreated with AAV, or 23-30 days after the last paclitaxel dosage for mice in post-chronic pain models.

Intrathecal BzATP injection: BzATP (2′(3′)-O-(4-Benzoylbenzoyl) adenosine 5′-triphosphate triethylammonium salt) was purchased from Millipore Sigma and, based on previous tests, was dissolved in saline (NaCl 0.9%) to final a concentration of 30 nmol. Saline solution was also used as a vehicle control and both were delivered in a 5 µL volume. Intrathecal injections were performed under isoflurane anesthesia (2.5%) by lumbar puncture with a 30-gauge needle attached to a Hamilton syringe.

Pain behavioral tests

Mice were habituated to the behavior and to the experimental chambers for at least 30 min before testing. As a positive comparator, gabapentin (Sigma, G154) was dissolved in saline solution and injected i.p. at 100 mg/kg one hour before behavioral testing.

Thermal Withdrawal Latency (Hargreaves Test): To determine the acute nociceptive thermal threshold, the Hargreaves' test was conducted using a plantar test device (Ugo Basile, Italy) *(79)*. Animals were allowed to freely move within a transparent plastic enclosure (6 cm diameter × 16 cm height) on a glass floor 40 min before the test. A mobile radiant heat source was then placed under the glass floor and focused onto the hind paw. Paw withdrawal latencies were measured with a cutoff time of 30 seconds. An IR intensity of 40 was employed. The heat stimulation was repeated three times on each hind paw with a 10 min interval to obtain the mean latency of paw withdrawal. The experimenter was blinded to composition of treatment groups.

Tactile allodynia: For the BzATP pain model, tactile thresholds (allodynia) were assessed 30 minutes, 1, 2, 3, 6, 24 hours after the BzATP injection. For the paclitaxel model, tactile thresholds (allodynia) were assessed 24 hours and 105 days after the last paclitaxel injection for mice pretreated with AAV, or 21-28 days after the last paclitaxel injection for mice that were first treated with paclitaxel and then with AAV after confirming chronic pain (post-chronic pain model). Forty-five minutes before testing, mice were placed in clear plastic wire mesh-bottom cages for acclimation. The 50% probability of withdrawal threshold was assessed using von Frey filaments (Seemes

Weinstein von Frey anesthesiometer; Stoelting Co.) ranging from 2.44 to 4.31 (0.04–2.00 g) in an up-down method, as previously described *(78)*.

Cold allodynia: Cold allodynia was measured by applying drops of acetone to the plantar surface of the hind paw as previously described *(71, 80)*. Mice were placed in individual plastic cages on an elevated platform and were habituated for at least 30 min until exploratory behaviors ceased. Acetone was loaded into a one mL syringe barrel with no needle tip. One drop of acetone (approximately 20 µL) was then applied through the mesh platform onto the plantar surface of the hind paw. Care was taken to gently apply the bubble of acetone to the skin on the paw without inducing mechanical stimulation through contact of the syringe barrel with the paw. Paw withdrawal time in a 60s observation period after acetone application was recorded. Paw withdrawal behavior was associated with secondary animal responses, such as rapid flicking of the paw, chattering, biting, and/or licking of the paw. Testing order was alternated between paws (right and left) until five measurements were taken for each paw. An interstimulation interval of 5 minutes was allowed between testing of right and left paws.

Tissue collection

Spinal cords were removed via hydroextrusion (injection of 2 mL of iced saline though a short blunt 20 gauge needle placed into the spinal canal following decapitation). After spinal cord tissue harvest, the L4-L6 DRG on each side were combined and frozen as for the spinal cord. Samples were placed in DNase/RNase-free 1.5 mL centrifuge tubes, quickly frozen on dry ice, and then stored at 80°C for future analysis.

Gene Expression Analysis and qPCR

RNA from Neuro2a cells was extracted using RNeasy Kit (QIAGEN; 74104) and from DRG using RNeasy Micro Kit (QIAGEN; 74004). cDNA was synthesized from RNA using Protoscript II Reverse Transcriptase Kit (NEB; E6560L). Real-time PCR (qPCR) reactions were performed using the KAPA SYBR Fast qPCR Kit (Kapa Biosystems; KK4601), with gene-specific primers in technical triplicates and in biological triplicates (Neuro2a cells), or in technical triplicates and biological replicates (various) for all in vivo studies. Relative mRNA expression was normalized to GAPDH and fold change was calculated using the comparative CT (ΔΔCT) method and normalized to GAPDH. Mean fold change and SD were calculated using Microsoft Excel And GraphPad Prism.

RNA-sequencing

RNA-Seq fastq files were mapped to GRCm38 and quantified read counts were mapped to each gene's exon using Ensembl v97 and STAR aligner *(81)*. The counts were then inputted to DESeq2 *(82)* for differential expression analysis, with log fold changes computed using the apeglm shrinkage estimator. Genes with an adjusted p-value less than 0.01 were considered to be significantly differentially expressed.

Toxicity/Side Effect Test Battery

Body weights. Body weights were recorded to the nearest 0.1g using a compact portable scale (#CB; Braintree Scientific).

Rectal body temperatures. Core body temperatures were measured using a digital thermometer (Body Temperature Thermometer, 50316, Stoelting Co.), with a mouse rectal probe (#RET; 3/4" length, 0.028" diameter; Braintree Scientific).

Grip strength test. Grip strength was measured with a mouse Grip Strength Meter (Columbus Instruments) according to the manufacturer's instructions (User Manual 0167-007). All-limb measurements were performed with the angled grid attachment, pulling the mouse towards the meter by the tail after engagement of all limbs. 5 consecutive measurements per mouse are taken and the highest 3 values are averaged, and data are expressed as newtons of peak force divided by the mouse's weight.

Rotarod test. A Rota-rod Series 8 apparatus (IITC Life Sciences) was used which records test results when the animal drops onto the individual sensing platforms below the rotating rod. Mice were subjected to an accelerating test strategy whereby the rod starts at 0 rpm and then accelerates at 10 rpm*(83, 84)*. The mice were tested in 3 set of 3 trials.

Marble burying. The marble burying test was used to assess anxiety-like *(85)* and possibly obsessive-compulsive-like behavior *(86)* capitalizing on a species-typical behavior of digging *(41)*. Importantly, this test appears to be able to capture the

anxiogenic-like behavior associated with painful states *(87, 88)*. Mice were placed individually in standard mouse cages containing bedding that is 5 cm in depth, with 20 small marbles arranged in 4 evenly spaced rows of 5 on top of the bedding material. After 30 min mice were removed and the number of marbles buried (at least 2/3 covered by bedding) is determined.

Nest building. Nest building is a natural rodent behavior that relates to reproduction, temperature regulation, shelter, and social behaviors. Approximately 1 h before the dark phase, mice were transferred to individual testing cages with wood-chip bedding but no environmental enrichment items such as paper towel. Nestlet material (3 g) was then placed in each cage. The nests were assessed at 2, 4, 6, 8, and 12 hr on a rating scale of 1–5 based on nest construction *(41)*. Mice were then returned to their original cages.

Olfactory test. This test examines the ability of a mouse to locate a desired food item buried under bedding. Mice were food restricted for 4 days (day 1- no food, day 2- 1.5 g food, day 3 & 4 – 1 g food + 1 piece chocolate puff cereal). Mice were monitored carefully, and body weights are recorded daily. On day 4 each mouse was placed in a clean cage with 2 inches bedding to habituate for 20 min. The mouse was removed, and a chocolate puff cereal was placed on top of the bedding. The mouse was then put back in the opposite end of the cage and the latencies to approach the pellet and manipulate the cereal were recorded. This test is primarily used to confirm that the mouse is motivated to find and eat the cereal. On day 5, the exact same procedure was used, but now the cereal piece is completely covered with bedding material. Again, latencies to locate and handle the cereal were recorded.

Cognitive test – Novel object recognition test. This test assays recognition memory while leaving the spatial location of the objects intact and is believed to involve the hippocampus, perirhinal cortex, and raphe nuclei *(89–91)*. The basic principle is that animals explore novel environments and that with repeated exposure decreased exploration ensues (habituation) *(92)*. A subsequent object substitution (replacing a familiar object with a novel object) results in dishabituation of the previously habituated exploratory behavior *(92, 93)*. The resulting dishabituation is expressed as a preferential exploration of the novel object relative to familiar features in the environment. This dishabituation has generally been interpreted as an expression of the animal's

recognition memory: the novel object is explored preferentially because it differs from what the animal remembers*(94)*. Mice were individually habituated to a 51cm x 51cm x 39cm open field for 5 min. Mice were then tested with two identical objects placed in the field (either two 250 ml amber bottles or two clear plastic cylinders 6x6x16cm half filled with glass marbles). An individual animal was allowed to explore for 5 min, now with the objects present. After two such trials (each separated by 1 minute in a holding cage), the mouse was tested in the object novelty recognition test in which a novel object replaces one of the familiar objects (for example, an amber bottle if the cylinders were initially used). All objects and the arena are thoroughly cleaned with 70% ethanol between trials to remove odors. Behavior is video recorded and then scored for contacts (touching with nose or nose pointing at object and within 0.5 cm of object). Habituation to the objects across the familiarization trials (decreased contacts) is an initial measure of learning and then renewed interest (increased contacts) in the new object indicates successful object memory.

H&E Staining

Two-month-old C57BL/6J male mice were injected i.t. with 1×10^{10}, 1×10^{11}, or 1×10^{12} vg/mouse of AAV9 mCherry or AAV9 Zinc-Finger-4. 21 Days following i.t. injections, mice were transcardially perfused with 4% PFA and lumbar DRG were post-fixed in 4% PFA for 24 hours, stored in PBS with 0.02% sodium azide, and sectioned using standard protocols.

Histopathology analysis

H&E stained paraffin sections (blinded to experimental condition), were reviewed independently by three neuropathologists. After independent review, the findings were reviewed in a group for discussion and to find points of consensus.

Multielectrode array recording

Action potential firing was measured using a multiwell MEA system (Maestro, Axion Biosystems). In each experiment, DRG neurons from male C57BL/6J were seeded in a 6-well MEA recording plate (2 wells for each animal). AAV was then added to each well at 1×10^{11} vg/well, and after sufficient recovery time, measurements were taken. The investigator was blinded to the identity of the virus added. To collect measurements, MEA plates were placed in the reader with the reader plate heater set to either 37℃ and

42℃ and under 95% O_2/5% CO_2 air flow. Plates were allowed to equilibrate to these conditions for a minimum of 5 minutes before collecting spontaneous recordings for 180 seconds. Electrical signals were collected and analyzed using the AxIS Software and Neural Metric Tool (Axion Biosystems) with Spontaneous Neural configuration. Signals were filtered with a band-pass filter of 200 Hz – 3 kHz. Spikes were detected with AxIS software using an adaptive threshold crossing set to 5.5 times the standard deviation of the estimated noise for each electrode.

RNAscope ISH Assays

The $Na_V1.7$ probe was designed by Advanced Cell Diagnostics (ACD Cat#313341) and was designed to detect detect 3404–4576 bp of the *Mus musculus* $Na_V1.7$ mRNA sequence (NM_018852.2, C3 channel). DRG were placed into paraffin, sectioned (12 µm thick), and mounted on positively charged microscopic glass slides (Fisher Scientific). All hybridization and amplification steps were performed following the ACD RNAscope V2 Formalin-Fixed Paraffin-Embedded (FFPE) sample preparation protocol. Cover slips were added on stained slides with fluorescent mounting medium (ProLong Gold Anti-fade Reagent P36930; Life Technologies) and scanned into digital images with a Zeiss 880 Airyscan Confocal at 20x magnification. Data was processed using ZEN software (manufacturer-provided software).

Quantification of RNAscope Signal. Full-size confocal images were converted to 8-bit greyscale in ImageJ. A universal threshold was applied across all images, and particles were counted. All particles with an area below 30 pixels were treated as representing a single probe. For particles of larger pixel area, the total pixel area was divided by 30 to obtain the approximate number of probes represented by a given particle. Individual DRG cells were identified via DAPI stains and counted manually to obtain the total number of DRG cells on each image. The average number of probes per cell was then obtained by dividing the total number of probes by the total number of DRG cells.

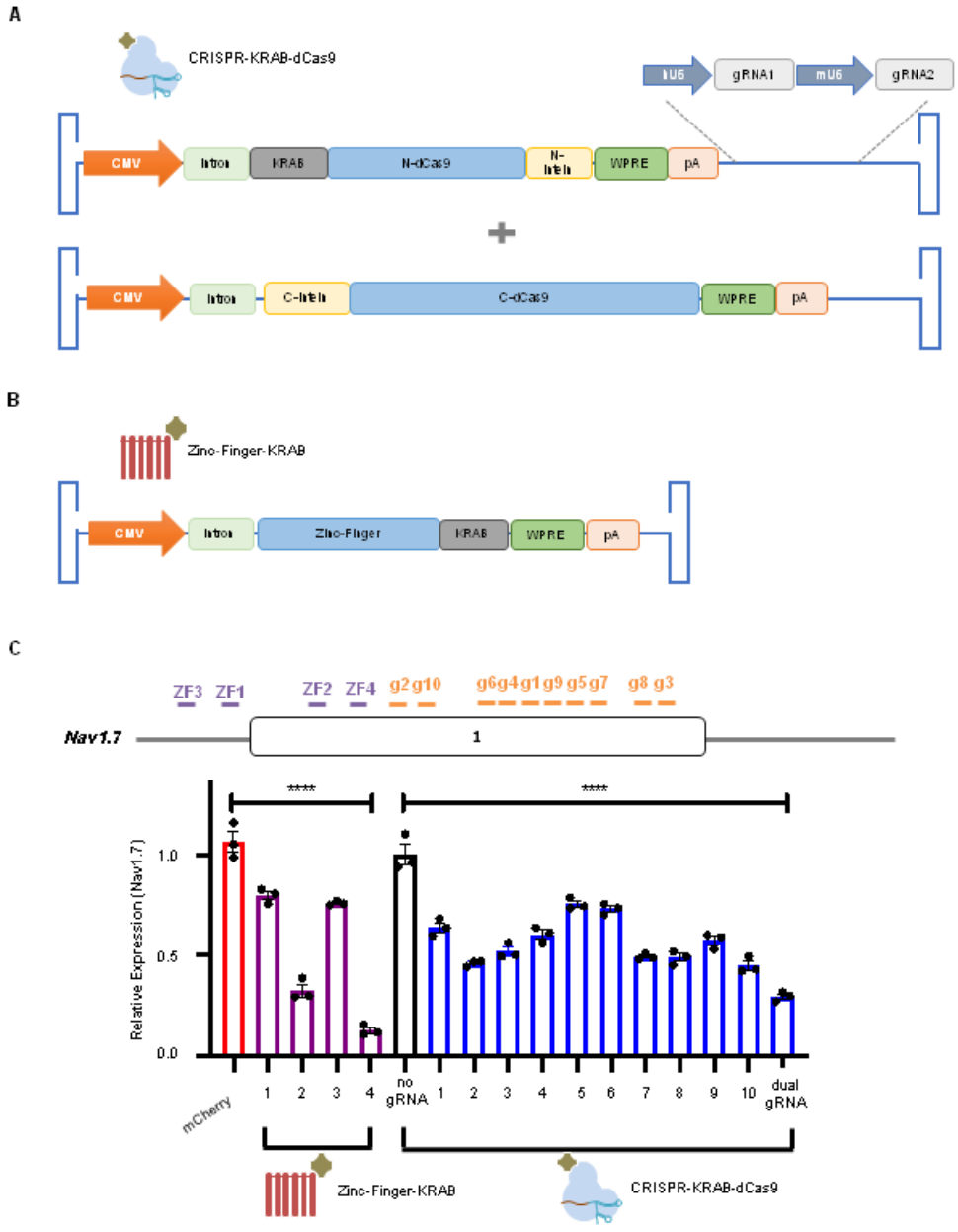

Fig. S1. In vitro optimization of epigenetic genome engineering tools to enable $Na_V1.7$ repression. (A) Schematic of a dual-pAAV intein-mediated split-*Streptococcus pyogenes* dead Cas9 (dCas9) for genome regulation. **(B)** Schematic of Zinc-Finger

pAAV for genome regulation. **(C)** A panel of four zinc finger proteins and ten gRNAs were designed to target $Na_V1.7$ in a mouse neuroblastoma cell line (Neuro2a) and were screened for repression efficacy by qPCR. A non-targeting gRNA (no gRNA) was used as a control for -dCas9 constructs targeting $Na_V1.7$, while mCherry was used as a control for ZFP-KRAB constructs targeting $Na_V1.7$ (dots represent individual biological replicates; qPCR was performed in technical triplicates; n=3; error bars are SEM; values normalized to Gapdh; one-way ANOVA with Dunnett's *post hoc* test; ****$p < 0.0001$).

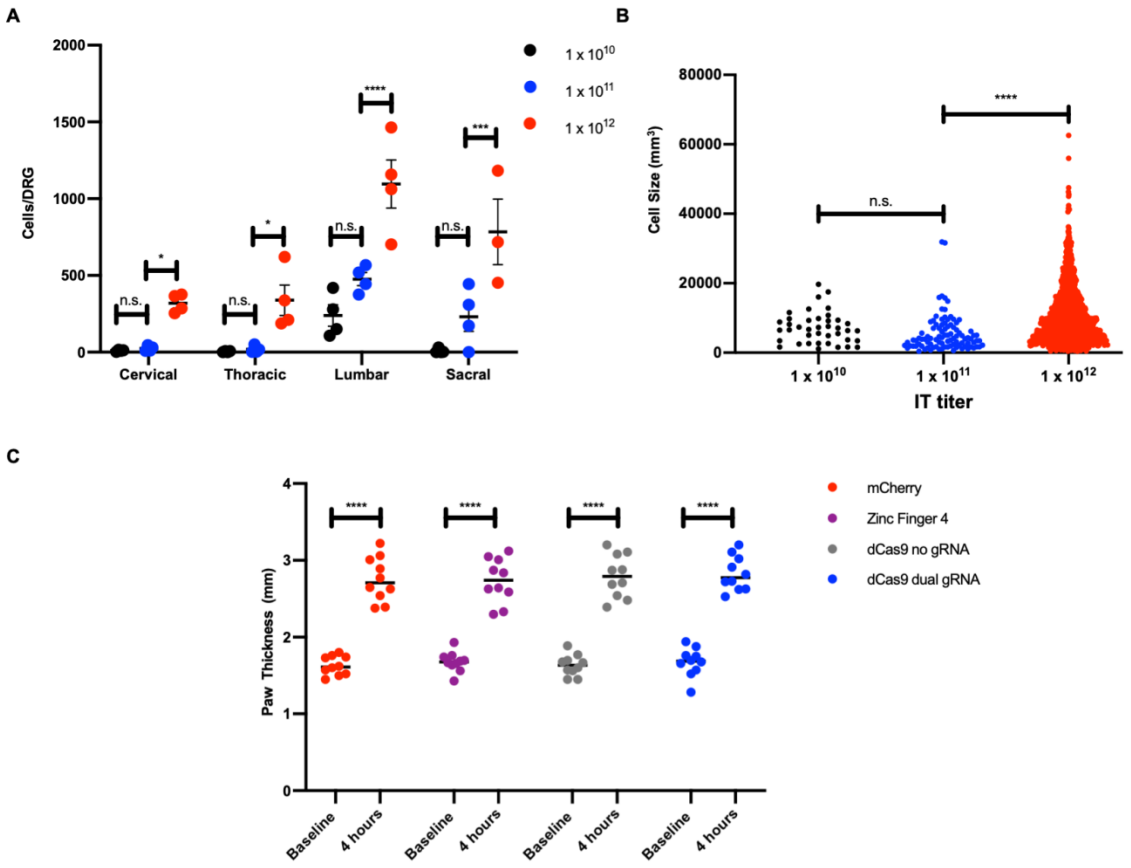

Fig. S2. Quantification of DRG transduction efficiencies via AAVs and carrageenan-induced inflammation in mice. (A) The number of mCherry positive cells in whole mount DRG (from Figure 2) along the neuroaxis following intrathecal injections of AAV9-mCherry illustrating transduction efficacy at different viral titers (1×10^{10}, 1×10^{11},

or 1×10^{12} vg/mouse; dots represent individual biological replicates; n=3-4; error bars are SEM; Two-way ANOVA with Bonferroni's *post hoc* test; n.s. = not significant, *p = 0.0384, *p = 0.0224, ****p < 0.0001; ***p = 0.0002). **(B)** The cell size distribution of mCherry positive cells in mice cervical DRG following intrathecal injections of AAV9-mCherry at different viral titers (1×10^{10}, 1×10^{11}, or 1×10^{12} vg/mouse) is quantified (dots represent individual cells; One-way ANOVA with Tukey's *post hoc* test; n.s. = not significant, ****p < 0.0001). **(C)** Paw thickness of ipsilateral paws at baseline and four hours after carrageenan injection are plotted (dots represent individual biological replicates; n=10; error bars are SEM; Student's t-test; ****p < 0.0001).

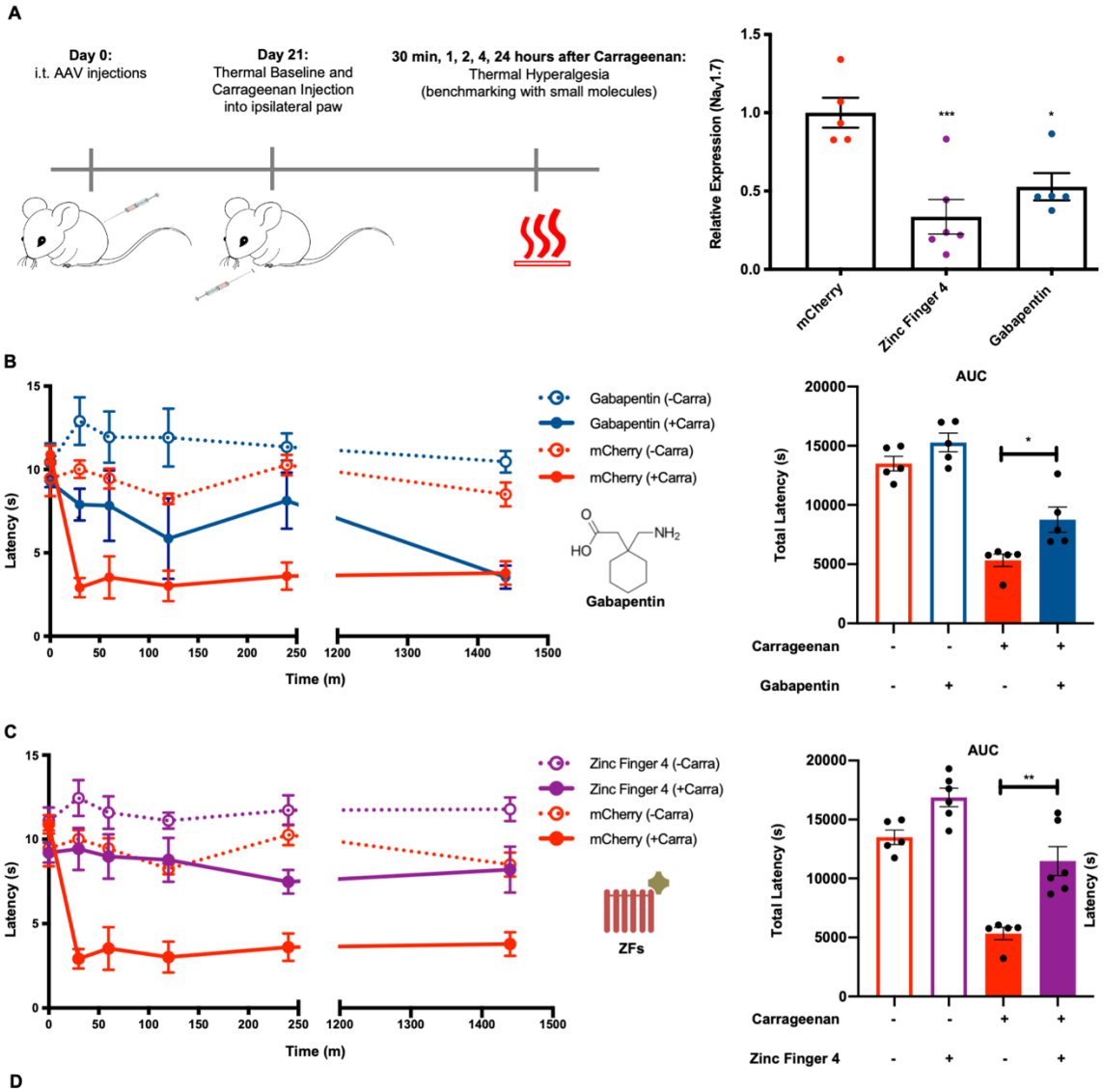

D

Comparison	Group	Pre-carrageenan	Post-carrageenan				
		0 minutes	30 minutes	1 hour	2 hours	4 hours	24 hours
mCherry (+Carra)	ZF-4-KRAB (+Carra)	n.s.	****p<0.0001	***p=0.0002	****p< 0.0001	*p=0.0104	**p=0.0028
	Gabapentin (+Carra)	n.s.	**p=0.0081	*p=0.0276	n.s.	*p=0.0184	n.s.
mCherry (-Carra)	ZF-4-KRAB (-Carra)	n.s.	n.s.	n.s.	n.s.	n.s.	n.s.
	Gabapentin (-Carra)	n.s.	n.s.	n.s.	n.s.	n.s.	n.s.

Fig. S3. Benchmarking of in situ repression of $Na_V1.7$ using ZFP-KRAB with established small-molecule drug gabapentin. (A) In vivo $Na_V1.7$ repression efficiencies from treated mice DRG. Twenty-four hours after carrageenan administration, mice DRG (L4-L6) were harvested and $Na_V1.7$ repression efficacy was determined by qPCR (dots represent individual biological replicates; n=5 for mCherry and gabapentin

groups, n=6 for Zinc-Finger-4-KRAB group; error bars are SEM; one-way ANOVA with Dunnett's *post hoc* test; ***p = 0.0007, *p = 0.0121). **(B,C)** Time course of thermal hyperalgesia after the injection of carrageenan (solid lines) or saline (dotted lines) into the hind paw of mice injected with gabapentin (100mg/kg), AAV9-mCherry and AAV9-Zinc-Finger-4-KRAB are plotted. Mean paw withdrawal latencies (PWL) are shown. The Area Under the Curve (AUC) of the thermal-hyperalgesia time-course are plotted on the right panels. A significant increase in PWL is seen in the carrageenan-injected paws of mice injected with gabapentin and Zinc-Finger-4-KRAB (dots represent individual biological replicates; n=5 for mCherry and gabapentin, n=6 for Zinc-Finger-4-KRAB; error bars are SEM; Student's t-test, *p = 0.0208, **p = 0.0021). **(D)** Significance of paw withdrawal latencies in mice receiving AAV9-Zinc-Finger-4-KRAB and gabapentin (100 mg/kg) as compared to AAV9-mCherry carrageenan-injected paw (negative control). Two-way ANOVA with Bonferroni *post hoc* test.

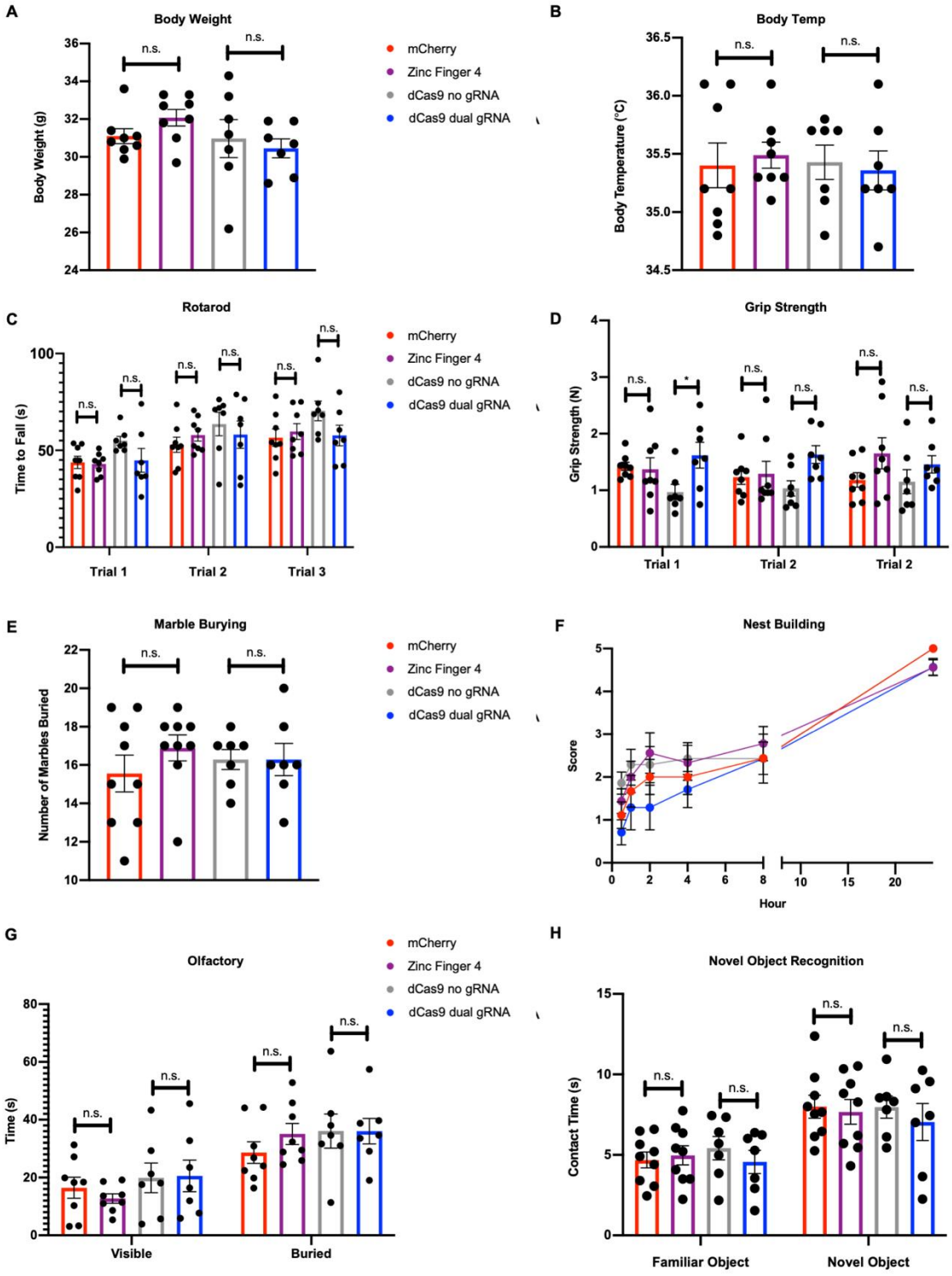

Fig. S4. Examining the safety of in situ repression of $Na_V1.7$ via ZFP-KRAB and KRAB-dCas9. (A) Body weight of mice injected with AAV9-mCherry, AAV9-Zinc-Finger-4-KRAB, AAV9-KRAB-dCas9-no-gRNA, and AAV9-KRAB-dCas9-dual-gRNA are plotted (dots represent individual biological replicates; n=8 for mCherry and Zinc-Finger-4

groups and n=7 for dCas9-no-gRNA and dCas9-dual-gRNA groups; error bars are SEM; Student's t-test; n.s. = not significant). **(B)** Body temperature of mice injected with AAV9-mCherry, AAV9-Zinc-Finger-4-KRAB, AAV9-KRAB-dCas9-no-gRNA, and AAV9-KRAB-dCas9-dual-gRNA are plotted (dots represent individual biological replicates; n=8 for mCherry and Zinc-Finger-4 groups and n=7 for dCas9-no-gRNA and dCas9-dual-gRNA groups; error bars are SEM; Student's t-test; n.s. = not significant). **(C)** Rotarod studies to determine motor coordination and balance of mice injected with AAV9-Zinc-Finger-4-KRAB and AAV9-KRAB-dCas9-dual-gRNA (dots represent individual biological replicates; n=8 for mCherry and Zinc-Finger-4 groups and n=7 for dCas9-no-gRNA and dCas9-dual-gRNA groups; error bars are SEM; Two-way ANOVA with Bonferroni *post hoc* test; n.s. = not significant). **(D)** No significant changes in grip strength was seen in mice injected with AAV9-mCherry, AAV9-Zinc-Finger-4, AAV9-KRAB-dCas9-no-gRNA, and AAV9-KRAB-dCas9-dual-gRNA (dots represent individual biological replicates; n=8 for mCherry and Zinc-Finger-4 groups and n=7 for dCas9-no-gRNA and dCas9-dual-gRNA groups; error bars are SEM; Two-way ANOVA with Bonferroni *post hoc* test; *p = 0.0402, n.s. = not significant). **(E)** The number of marbles buried by mice injected with AAV9-mCherry, AAV9-Zinc-Finger-4, AAV9-KRAB-dCas9-no-gRNA, and AAV9-KRAB-dCas9-dual-gRNA are plotted (dots represent individual biological replicates; n=8 for mCherry and Zinc-Finger-4 groups and n=7 for dCas9-no-gRNA and dCas9-dual-gRNA groups; error bars are SEM; Student's t-test; n.s. = not significant). **(F)** Nest building scores demonstrated no significant changes between experimental and control groups (dots represent individual biological replicates; n=8 for mCherry and Zinc-Finger-4 groups and n=7 for dCas9-no-gRNA and dCas9-dual-gRNA groups; error bars are SEM; Two-way ANOVA with Bonferroni *post hoc* test). **(G)** An olfactory test was performed to determine whether knockdown of $Na_V1.7$ via AAV9-Zinc-Finger-4-KRAB and AAV9-KRAB-dCas9-dual-gRNA causes anosmia. No significant olfactory detection changes were seen in mice injected with AAV9-Zinc-Finger-4-KRAB and AAV9-KRAB-dCas9-dual-gRNA as compared to the control groups, AAV9-mCherry and AAV9-KRAB-dCas9-no gRNA, respectively (dots represent individual biological replicates; n=8 for mCherry and Zinc-Finger-4 groups and n=7 for dCas9-no-gRNA and dCas9-dual-gRNA groups; error bars are SEM; One-way ANOVA with Bonferroni *post hoc* test; n.s. = not significant). **(H)** A novel object recognition test showed comparable memory retention in mice injected with AAV9-Zinc-Finger-4-KRAB and AAV9-KRAB-dCas9-dual-gRNA as compared to the control groups, AAV9-mCherry and AAV9-KRAB-dCas9-no gRNA,

respectively (dots represent individual biological replicates; n=8 for mCherry and Zinc-Finger-4 groups and n=7 for dCas9-no-gRNA and dCas9-dual-gRNA groups; error bars are SEM; One-way ANOVA with Bonferroni *post hoc* test; n.s. = not significant).

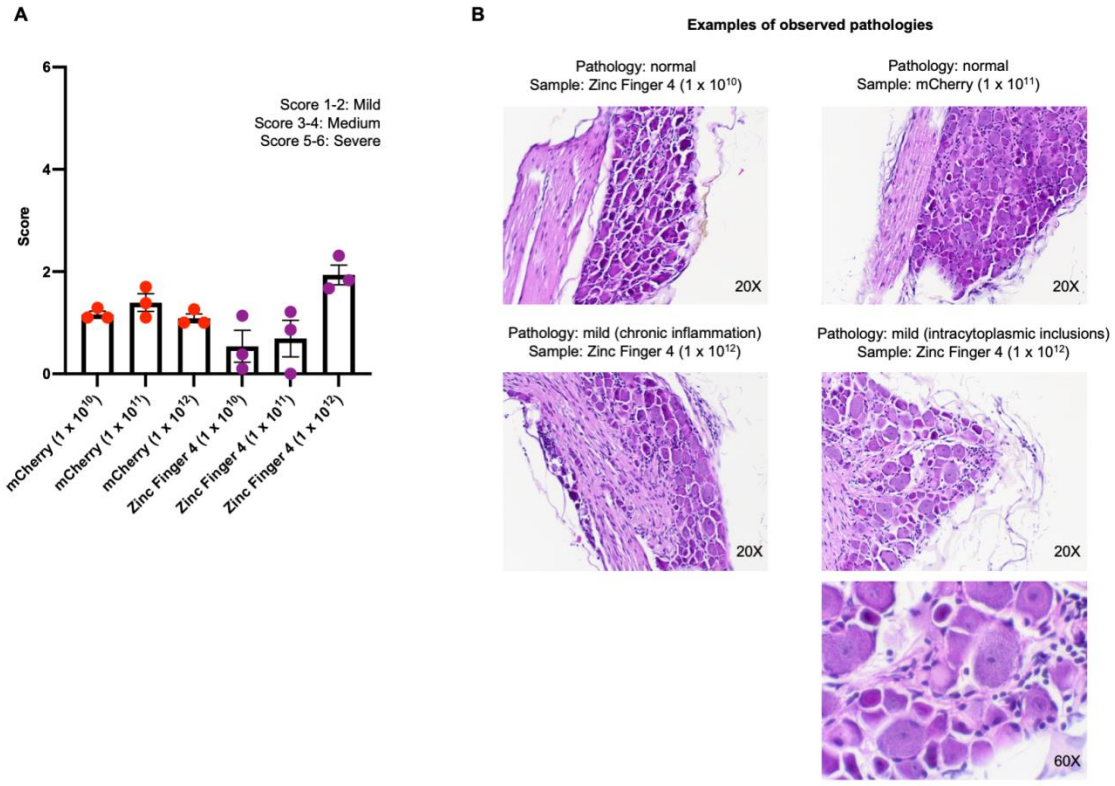

Fig. S5. Neuropathology analyses of DRGs targeted via AAVs. (A) H&E stained paraffin sections (blinded to experimental condition), were reviewed independently by three neuropathologists. After independent review, the findings were reviewed in a group

for discussion and to find points of consensus. In all cases, the DRGs showed no loss of neurons, and the nerves showed no axonal injury or myelin pathology (dots represent individual biological replicates; n=3; error bars are SEM). **(B)** In one case, DRG neurons showed intracytoplasmic inclusions of unknown significance (image depicted in panel b). In another case, focal mild chronic inflammation was seen (image depicted in panel b). These two cases also scored highest on semiquantitative pathology scoring. Other cases appeared normal (representative images depicted in panel b) or showed only mild or questionable findings (such as questionable mild nerve edema).

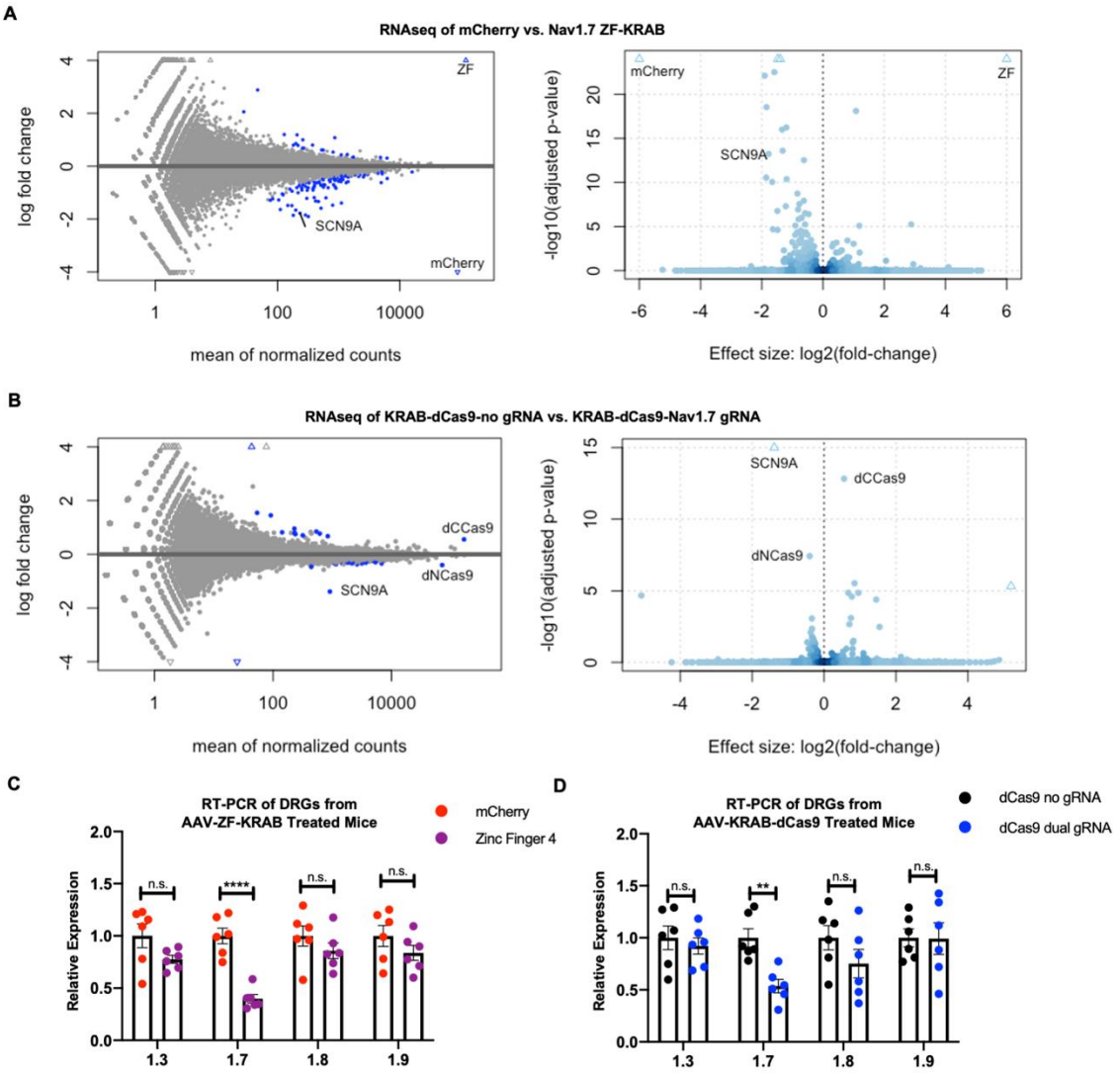

Fig. S6. Genome-wide analysis of gene expression in zinc finger or CRISPR-treated Neuro2a cells. (A) Blue data points indicate FDR < 0.01 by differential-expression analysis (n = 3 for Neuro2a). The data points representing the ZF and mCherry transcripts are highlighted as blue triangles. **(B)** Blue data points indicate FDR < 0.01 by differential-expression analysis (n = 3 for Neuro2a). The data points representing the dNCas9 and dCCas9 are highlighted as blue triangles **(C)** Following paclitaxel administration and i.t. AAV9 delivery (Fig. 4), mice DRG (L4-L6) were harvested and $Na_V1.3$, $Na_V1.7$**,** $Na_V1.8$, and $Na_V1.9$ expression relative to Gapdh were determined by qPCR in mice injected with AAV9-mCherry or AAV9-Zinc-Finger-4-KRAB (dots represent individual biological replicates; n=6; error bars are SEM; Student's t-test; ****p < 0.0001, n.s. = not significant). **(D)** Following paclitaxel administration and i.t. AAV9 delivery (Fig. 4), mice DRG (L4-L6) were harvested and $Na_V1.3$, $Na_V1.7$ **,** $Na_V1.8$,

and $Na_V1.9$ expression relative to Gapdh were determined by qPCR in mice injected with AAV9-KRAB-dCas9-no-gRNA or AAV9-KRAB-dCas9-dual-gRNA (dots represent individual biological replicates; n=6; error bars are SEM; Student's t-test; **p = 0.0092, n.s. = not significant).

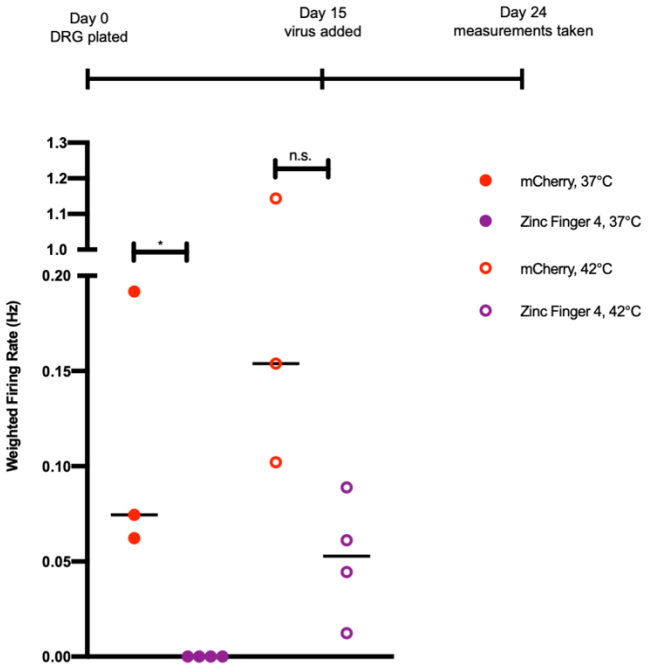

Fig. S7. Multielectrode array recordings of DRG neurons transduced with AAV9-Zinc-Finger-4 show reduced response to heat. Weighted firing rate from DRG transduced with AAV9-mCherry or AAV9-Zinc-Finger-4-KRAB is graphed (dots represent individual biological replicates; n=3 AAV9 mCherry and n=4 for AAV9 Zinc-Finger-4-KRAB transduced wells; Student's t-test; *p = 0.0248; n.s. = not significant).

Table S1. CRISPR-Cas9 gRNA spacer sequences.

gRNA	Sequence
SCN9A-1	ACAGTGGGCAGGATTGAAA
SCN9A-2	GAGCTCAGGGAGCATCGAGG
SCN9A-3	GCAGGTGCACTCACCGGGT
SCN9A-4	AGAGTCGCAATTGGAGCGC
SCN9A-5	CCAGACCAGCCTGCACAGT
SCN9A-6	GAGCGCAGGCTAGGCCTGCA
SCN9A-7	CTAGGAGTCCGGGATACCC
SCN9A-8	GAATCCGCAGGTGCACTCAC
SCN9A-9	GACCAGCCTGCACAGTGGGC
SCN9A-10	GCGACGCGGTTGGCAGCCGA

Table S2. ZFP genomic target sequences.

ZF Name	ZF Target Sequence	ZF Protein Sequence
ZF1	GGCGAGGTGATGGAAGGG	RSMHDYKDHDGDYKDHDIDY KDDDDKMAPKKKRKVGIHGV PAAMAERPFQCRICMRNFSR SAHLSRHIRTHTGEKPFACD ICGRKFAQSGNLARHTKIHT GSQKPFQCRICMRNFSRSDA MSQHIRTHTGEKPFACDICG RKFARNASRTRHTKIHTGSQ KPFQCRICMRNFSRSANLAR HIRTHTGEKPFACDICGRKF ADRSHLARHTKIHLRQKDAA RGSRTLVTFKDVFVDFTREE WKLLDTAQQIVYRNVMLENY KNLVSLGYQLTKPDVILRLE KGEEPWLVDYKDDDDKRS
ZF2	GAGGGAGCTAGGGGTGGG	RSMHDYKDHDGDYKDHDIDY KDDDDKMAPKKKRKVGIHGV PAAMAERPFQCRICMRNFSR SANLARHIRTHTGEKPFACD ICGRKFADSSDRKKHTKIHT GSQKPFQCRICMRNFSTSGS LSRHIRTHTGEKPFACDICG RKFAHSLSLKNHTKIHTGSQ KPFQCRICMRNFSQSSDLSR HIRTHTGEKPFACDICGRKF AWKWNLRAHTKIHLRQKDAA RGSRTLVTFKDVFVDFTREE WKLLDTAQQIVYRNVMLENY KNLVSLGYQLTKPDVILRLE KGEEPWLVDYKDDDDKRS
ZF3	AGTGCTAATGTTTCCGAG	RSMHDYKDHDGDYKDHDIDY KDDDDKMAPKKKRKVGIHGV PAAMAERPFQCRICMRNFSR SAHLSRHIRTHTGEKPFACD ICGRKFATSGHLSRHTKIHT GSQKPFQCRICMRNFSRSDH LSQHIRTHTGEKPFACDICG RKFAASSTRTKHTKIHTGSQ KPFQCRICMRNFSQSSHLTR HIRTHTGEKPFACDICGRKF ARSDNLTRHTKIHLRQKDAA RGSRTLVTFKDVFVDFTREE WKLLDTAQQIVYRNVMLENY

		KNLVSLGYQLTKPDVILRLE KGEEPWLVDYKDDDDKRS
ZF4	TAGACGGTGCAGGGCGGA	RSMHDYKDHDGDYKDHDIDY KDDDDKMAPKKKRKVGIHGV PAAMAERPFQCRICMRNFSD RSHLTRHIRTHTGEKPFACD ICGRKFADRSHLARHTKIHT GSQKPFQCRICMRNFSRSDN LSEHIRTHTGEKPFACDICG RKFARSAALARHTKIHTGSQ KPFQCRICMRNFSRSDTLSQ HIRTHTGEKPFACDICGRKF ATRDHRIKHTKIHLRQKDAA RGSRTLVTFKDVFVDFTREE WKLLDTAQQIVYRNVMLENY KNLVSLGYQLTKPDVILRLE KGEEPWLVDYKDDDDKRS

Table S3. qPCR primers.

Gene	Forward	Reverse
Gapdh	TGGCCTTCCGTGTTCCTAC	GAGTTGCTGTTGAAGTCGCA
Scn3a	GGGCCTTCTTATCGCTGTTTCG	CCCAGCTGCACGTAATGTCAAC
Scn9a	GGCAGAAGCTGAGCCTATCAATGC	TGGAAATCTCCTCACACAGCCATC
Scn10a	TTTCCGAGCACAGAGGGCAATG	CAGCTTAGACTCTTCCAGCTCCTC
Scn11a	TTCTTGGCTTCCCTCAGAGTGC	GTGTTTAATGTGGGCCAGGATTTG